A focus on critical aspects of uptake and transport of milk-derived extracellular vesicles across the Caco-2 intestinal barrier model

Josepha Roerig[a], Laura Schiller[b], Hermann Kalwa[c], Gerd Hause[d], Cica Vissiennon[b], Michael C. Hacker[a,e], Christian Wölk[a], Michaela Schulz-Siegmund[a,*]

[a]Pharmaceutical Technology, Institute of Pharmacy, Medical Faculty, Leipzig University, Germany

[b]Institute of Medical Physics and Biophysics, Medical Faculty, Leipzig University, Germany

[c]Rudolf Boehm Institute of Pharmacology and Toxicology, Medical Faculty, Leipzig University, Germany

[d]Biocenter, Martin Luther University Halle-Wittenberg, Germany

[e]Institute of Pharmaceutics and Biopharmaceutics, Heinrich-Heine University Düsseldorf, Germany

Abstract

Bovine milk-derived extracellular vesicles (EVs) hold promises as oral drug delivery systems. Since EV bioavailability studies are difficult to compare, key factors regarding EV uptake and intestinal permeability remain little understood. This work aims to critically study uptake and transport properties of milk-derived EVs across the intestinal barrier *in vitro* by standardization approaches.

Therefore, uptake properties were directly compared to liposomes in intestinal Caco-2 cells. Reliable staining results were obtained by the choice of three distinct EV labeling sites, while non-specific dye transfer and excess dye removal were carefully controlled. A novel fluorescence correction factor was implemented to account for different labelling efficiencies. Both EV and liposome uptake occurred mainly energy dependent with the neonatal Fc receptor (FcRn) providing an exclusive active pathway for EVs. Confocal microscopy revealed higher internalization of EVs whereas liposomes rather remained attached to the cell surface. Internalization could be improved when changing the liposomal formulation to resemble the EV lipid composition. In a Caco-2/HT29-MTX co-culture liposomes and EVs showed partial mucus penetration.

For transport studies across Caco-2 monolayers we further established a standardized protocol considering the distinct requirements for EVs. Especially insert pore sizes were systematically compared with 3 µm inserts found obligatory. Obtained apparent permeability coefficients (P_{app}) reflecting the transport rate will allow for better comparison of future bioavailability testing.

Graphical abstract

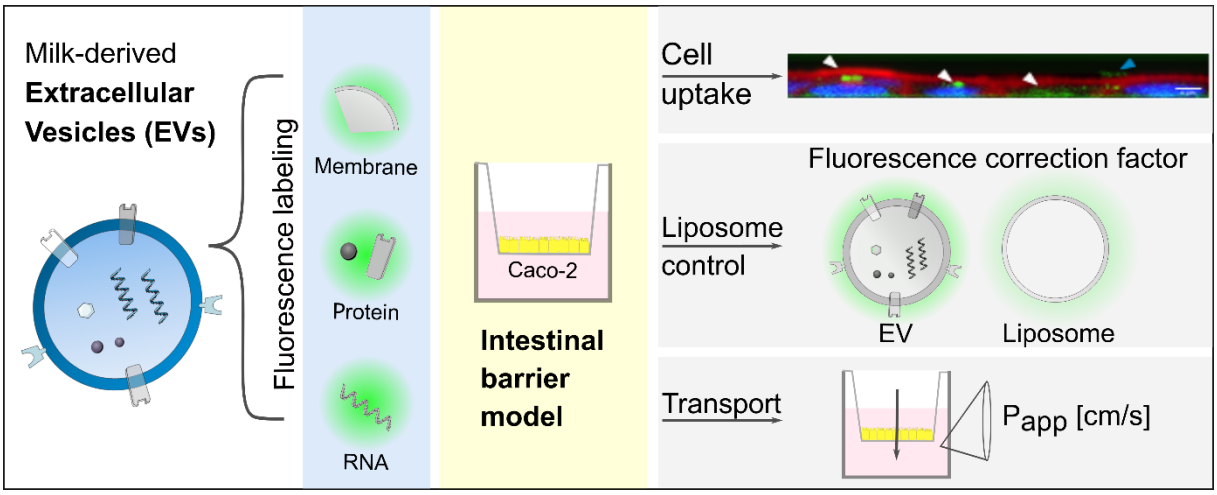

Keywords

Extracellular vesicles; bovine milk; liposomes; cell uptake; intestinal permeability; apparent permeability coefficient P_{app}

* Corresponding author

Michaela Schulz-Siegmund, schulz@uni-leipzig.de, Tel.: +49–341–9711900

1. Introduction

Oral drug delivery is considered a patient-friendly therapeutic intervention. Self-administration, dosing flexibility, storage capability, and patient compliance are among the benefits. However, oral delivery reaches its limitations for biological macromolecules e.g. peptides, proteins, and nucleic acid-based drugs. Harsh conditions of the gastrointestinal (GI) system including enzymatic and acidic degradation and low uptake across the intestinal barrier remain challenges for these biological therapeutics [1,2].

Liposomes were being investigated as drug delivery systems for decades and are already established in clinical use [3–5]. Though liposomes can encapsulate drug molecules, market-authorized formulations do not cover oral applications so far [6].

Bovine milk-derived extracellular vesicles (EVs) might help to overcome these obstacles. EVs are heterogenous cell-derived, membrane-enclosed structures in the nanometer size range. Once considered as cell debris, EVs are now recognized for their natural role in intercellular communication as they are known to shuttle nucleic acids (e.g. miRNA) between cells [7,8]. Especially bovine milk-derived EVs gain rising interest for oral drug delivery purposes due to their GI stability [9,10]. Their

abundance in nutritional milk and their lack of toxicity in *in vivo* studies [11,12] make them considerably safe for oral administration. The low-cost scalability of bovine milk-derived EVs presents an additional advantage compared to cell culture-derived EVs [13].

First evidence from literature indicates the uptake of bovine milk-derived EVs by intestinal cells [14]. Bioavailability was assessed in mice after oral gavage [9,15,16]. As bovine milk-derived EVs need to rely on post-isolation labeling strategies the remaining question is whether labeled EVs or (dissociated) dye are observed [17,18] limiting the comparability of bioavailability studies. Recent advances were made using a ^{99m}Tc (IV) label for single photon emission computed tomography (SPECT) imaging of EVs in mice [19]. Another approach is a click chemistry-based surface protein labeling [20].

In this study, we faced this issue of EV labeling by comparing different labeling sites including the EV membrane, intravesicular proteins, and RNA while controlling for non-specific dye transfer and excess dye removal. To further enhance the comparability of EV bioavailability studies we wanted to both characterize and standardize EV bioavailability *in vitro* regarding the two aspects: cell uptake and transport.

Firstly, direct comparisons with liposomes were performed to clarify if EVs can meet the high expectations of superior uptake properties compared to existing delivery systems. Therefore, a fluorescence correction factor was established which normalizes different labelling efficiencies. Polarized Caco-2 cells served as a model to mimic the intestinal barrier [21,22]. Differences regarding energy-dependent and non-energy-dependent uptake between EVs and liposomes were studied. Previously, the neonatal Fc receptor (FcRn) was reported to be involved in EV bioavailability in mice by Betker et. al. [16]. As the FcRn expression is known to vary among species, we validated the results in human cells for the first time. Non-energy-dependent internalization was investigated by changing the liposomal formulation to mimic the EV lipid composition (EVmL). Though Caco-2 cells are an established cell culture model for resorption studies of the upper intestine, the intestinal mucosa presents another significant barrier for nanoparticles after oral administration. We approached the mucus penetration of EVs and liposomes in a co-culture model of Caco-2 and goblet-like HT29-MTX cells [23].

Secondly, a standard protocol for *in vitro* transport studies across the Caco-2 monolayer was developed, thus allowing for faster screening of oral EV drug delivery in the future. Therefore, standard protocols published for small molecules [24,25] were carefully evaluated and adapted for EV purposes including a systematic comparison of insert pore sizes which appeared as a critical parameter for valuable transport experiments. Apparent permeability coefficients (P_{app}) reflecting the transport rate were calculated as a comparable unit for prospect, standardized intestinal permeability testings.

2. Methods and Materials

2.1 Materials

1,2-dipalmitoyl-*sn*-glycero-3-phosphocholine (DPPC), 1,2-dioleoyl-*sn*-glycero-3-phosphocholine (DOPC), 1,2-dioleoyl-*sn*-glycero-3-phophoethanolamine (DOPE), 1,2-dioleoyl-*sn*-glycero-3-phospho-L-serine (sodium salt) (DOPS) and sphingomyelin (SM) were purchased from Avanti® Polar Lipids, Inc. (Alabaster, USA). Dulbecco's Phosphate Buffered Saline (PBS) was purchased from Biowest (Riverside, USA). Further chemicals were purchased from Sigma-Aldrich (Steinheim, Germany) if not stated differently.

2.2 EV isolation

Bovine raw milk was purchased (Agrarprodukte Kitzen eG, Grosszschocher, Germany) and further processed within 24 hours. A differential centrifugation protocol was applied to 20 mL raw milk starting with 3,000 rcf to remove milk fat and cells followed by 12,000 rcf and three repetitions at 20,000 rcf using an Allegra 64R centrifuge with a F0630 fixed-angle rotor (Beckmann Coulter GmbH, Krefeld, Germany).

18 mL supernatant was loaded onto a HiPrep 26/60 Sephacryl S-500 HR (GE Healthcare, USA) column via a 50 mL Superloop™ (GE Healthcare, USA) connected to an ÄKTApurifier system (GE Healthcare, USA). PBS pH 7.4, 20 mM EDTA was used as an elution buffer and fractions of 3 mL or 10 mL respectively were collected as described by Blans et al. [26]. Absorbance was measured at 280 nm to monitor the eluting fractions. All steps were performed at +4 °C.

To detect EV marker proteins according to the MISEV 2018 guidelines [7] nitrocellulose membranes (Bio-Rad, USA) were loaded with 5 µL aliquots of the eluting fractions diluted 1:1 in RIPA buffer as reported by Westergard et al. [27]. The membranes were blocked with 5% bovine serum albumin (BSA) in TBS-T buffer (1.37 M NaCl, 27 mM KCl, 0.25 M Tris pH 7.6, 0.5% Tween 20) at room temperature. Primary antibodies against the transmembrane proteins (category 1a/1b, MISEV 2018) CD63 (1:2000) and CD9 (1:1000), the cytosolic protein (category 2a) TSG101 (1:2000) and the milk whey contaminant (category 3) casein (1:2000) were added at respective dilutions. After incubation with corresponding HRP-labeled secondary antibodies (1:5000) and ECL-reagent, chemiluminescence was detected (G:Box, Syngene, UK). Purchased antibodies include mouse anti-CD63 (MCA2042GA, Bio-Rad, USA), mouse anti-CD9 (312102, BioLegend, USA), rabbit anti-TSG101 (ab125011, Abcam, UK), rabbit anti-casein (ab166596, Abcam, UK), goat anti-rabbit IgG-HRP (A16096, Invitrogen, USA), goat anti-mouse IgG-HRP (STAR207P, Bio-Rad, USA).

Fractions containing EV marker proteins and lowest casein concentrations were pooled and used for further studies.

2.3 Transmission Electron Microscopy (TEM) with negative staining

EVs were diluted with PBS to 0.05 mg · mL^{-1} adjusted to the protein concentration. The negatively stained samples were prepared by spreading the dispersion (5 µL) onto a Cu grid coated with a formvar film. After 1 min, excess liquid was removed by blotting with filter paper. After washing with H_2O the samples were stained with 2% aqueous uranyl acetate. The dried specimens were examined using an EM 900 transmission electron microscope (Carl Zeiss Microscopy GmbH, Oberkochen, Germany). Micrographs were acquired using an SSCCD SM-1k-120 camera (TRS, Moorenweis, Germany).

2.4 Cryo Transmission Electron Microscopy (CryoTEM)

Vitrified specimens for CryoTEM were prepared using a blotting procedure, performed in a chamber with controlled temperature and humidity using an EM GP grid plunger (Leica, Wetzlar, Germany). The sample dispersion (6 µL) was placed onto an EM grid coated with a holey carbon film (Cflat, Protochips Inc., Raleigh, NC, USA). Excess solution was then removed by blotting (12 s) with a filter paper to leave a thin film of the dispersion spanning the holes of the carbon film on the EM grid. Vitrification of the thin film was achieved by rapid plunging of the grid into liquid ethane held just above its freezing point. The vitrified specimen was kept below 108 K during storage, transferred to the microscope, and investigated.

Specimens were examined with a Libra 120 Plus transmission electron microscope (Carl Zeiss Microscopy GmbH, Oberkochen, Germany), operating at 120 kV. The microscope was equipped with a Gatan 626 cryotransfer system. Images were acquired using a BM-2k-120 dual-speed on-axis SSCCD camera (TRS, Moorenweis, Germany).

2.5 Bradford assay for protein concentration

The total protein content was determined using a Bradford assay (Bio-Rad, USA) with serial dilutions of BSA as a standard. Absorbance was measured at 610 nm (Synergy H1, BioTek, USA).

2.6 Sulpho-phospho-vanillin (SPV) assay for lipid concentration

The estimation of the total lipid content was performed as described by Visnovitz et al. [28]. In brief, a serial dilution of DOPC liposomes prepared in elution buffer was used as standards. Addition of 96% sulphuric acid and a phospho-vanillin reagent (1 mg · mL^{-1} vanillin in 17% phosphoric acid) resulted in a concentration dependent colorimetric reaction and absorbance was measured at 540 nm (Synergy H1, BioTek, USA).

2.7 Nanoparticle Tracking Analysis (NTA)

Nanoparticle tracking analysis was performed to determine the particle size distribution and particle concentration of all samples. A NanoSight LM10 (Malvern Panalytical Ltd, UK) equipped with a 488 nm laser was used. After setting the camera level to 12, three videos of 60 seconds were recorded in light scatter mode. For analysis, the NTA 3.1 software was used with the detection threshold set to 5. Software settings were kept constant for all measurements. Samples were diluted in particle-free PBS prior to analysis. As a parameter for the width of the size distribution a relative standard deviation (RSD) was calculated from the mean size and the standard deviation (SD) reported by the NTA 3.1 software. This can be correlated to a narrow (≤ 0.1), moderate (0.1 – 0.4), or polydisperse (≥0.4) size distribution (see Technical Notes, Malvern Panalytical Ltd, UK).

2.8 Liposome preparation

Standard liposomes were prepared based on market-authorized formulations [3] with DPPC and Cholesterol (Chol) at a molar ratio of 70/30. EV mimicking liposomes (EVmL) were prepared according to Lu et al. [29] with DOPC/SM/Chol/DOPS/DOPE at a molar ratio of 21/17.5/30/14/17.5. Thin film hydration was used to prepare the liposomal formulations. For this purpose, lipids were dissolved in chloroform/methanol (8:2) and organic solvent evaporated at 500 mbar for 30 min and at ≤ 20 mbar for further 90 min. The film was hydrated with sterile PBS pH 7.4 at +50 °C for 30 min under vigorous shaking. After treatment in an ultrasonic bath for 5 min the lipid mixture was extruded 21 x through a 200 nm pore sized polycarbonate membrane using a LiposoFast extruder (Avestin, Ludwigshafen, Germany) to obtain uniformly sized liposomes.

2.9 Electrophoretic Light Scattering (ELS) measurement

The zeta potential of three independent preparations of EVs, EV mimicking liposomes, and DOPC-Chol liposomes ($n = 3$) was determined with a Litesizer™ 500 (Anton Paar GmbH, Graz, Austria) using electrophoretic light scattering (ELS). After appropriate dilution in PBS samples were transferred to a Univette Cuvette (Anton Paar GmbH, Graz, Austria). The electrophoretic mobility μ was then measured after 60 seconds of equilibration time at +25 °C at an automatic voltage adjustment of 5.0 V. 100 runs were performed in series mode with three repetitions and the zeta potential ζ calculated according to the Smoluchowski equation using the Kalliope™ software (Anton Paar GmbH, Granz, Austria) provided with the instrument. The following parameters were assumed: solvent refractive index: 1.3303, solvent viscosity: $\eta = 0.8903$ mPa · s, solvent relative permittivity: $\varepsilon_r = 78.37$.

2.10 Fluorescence labeling

EVs were incubated with either 5 µM Vybrant DiO (Thermo Fisher, USA) for membrane labeling, 20 µM CellTrace CFSE (Thermo Fisher, USA) for intravesicular protein labeling, or 10 µM SYTO® RNASelect™ (Thermo Fisher, USA) for RNA labeling. Excess dye was removed with Vivaspin-500 300 kDa MWCO ultrafiltration columns (Sartorius, Germany). Labeled EVs were washed thrice with PBS. Washing controls were prepared with PBS instead to evaluate the excess dye removal.

The same protocol was applied for liposomes (DPPC-Chol and EVmL) labeled with DiO. To account for different affinities of the lipophilic DiO to the liposome or EV membrane a fluorescence correction factor was established. Labeled liposomes and EVs from three independent experiments each (n = 3) were adjusted to the same particle concentration after NTA measurement. The fluorescence intensities of liposomes (RFU_{Lipo}) and EVs (RFU_{EV}) were measured with a plate reader at $\lambda_{ex/em}$ = 487 / 523 nm at three different concentrations and a fluorescence correction factor was calculated as follows:

Fluorescence correction factor = RFU_{Lipo} / RFU_{EV} (equation 1).

2.11 Cell culture

Enterocyte-like Caco-2 cells (ACC 169, DMSZ, Braunschweig, Germany) and goblet cell-like HT29-MTX-E12 cells (12040401, Sigma-Aldrich partnered with ECACC Public Health England, Salisbury, UK) were cultured in Dulbecco's Modified Eagle's Medium (DMEM) high glucose supplemented with 10% fetal bovine serum (FBS), 1% penicillin-streptomycin (P/S) and 1% MEM non-essential amino acids (NEAA) (Biowest, USA) in a humidified atmosphere at +37 °C and 5% CO_2. For uptake experiments, Caco-2 cells or Caco-2 and HT29-MTX-E12 cells (ratio 9:1) respectively were seeded in PET transwell inserts with 33,000 cells per insert and a 0.4 µm pore size (Sarstedt, Nümbrecht, Germany) in a 24-well plate. After pre-tests with 0.4 / 1 / 3 µm inserts, Caco-2 cells were seeded in PET transwell inserts with 3 µm pores for transport studies (Sarstedt, Nümbrecht, Germany). Cell culture medium was changed three times per week. Caco-2 and HT29-MTX-E12 cells were used within a passage interval of maximum 5 passages.

Differentiation over 21 days was monitored every week with an EVOM² epithelial volt-ohmmeter and a STX3 chopstick electrode (World Precision Instruments, Friedberg, Germany). The Transepithelial Electrical Resistance (TEER) was then calculated based on the following equation:

$TEER\ [\Omega \cdot cm^2] = (R - R_b) \cdot A$ (equation 2).

R in this equation represents the resistance of inserts with cells, R_b is the resistance of inserts without cells, and A is the surface area of the inserts. We defined TEER values of 320 (± 65) Ω · cm² at +37 °C as acceptable. Cell monolayers with TEER values below 255 Ω · cm² were excluded from further

experiments. 24 hours before the experiments FBS was replaced by Panexin NTA (PAN Biotech, Germany) as a vesicle-free serum substitute.

Cell viability of Caco-2 cells incubated with EVs for up to 24 hours was assessed with Rotitest®Vital (Carl Roth, Karlsruhe, Germany) according to the manufacturer's instructions. Absorbance was measured at 450 nm and normalized to non-treated Caco-2 cells (n = 3).

Alcian Blue staining was used to visualize the presence of acidic mucins in Caco-2/HT29-MTX-E12 co-cultures after 21 days of differentiation as described by Béduneau et al. [30]. All experiments were run with n = 4, if not stated differently.

2.12 EV uptake by recipient cells

Cell uptake was performed under serum-free conditions with $2 \cdot 10^{11}$ particles per well. Differentiated Caco-2 cells were incubated with fluorescently labeled EVs for 15 min up to 24 hours. For dye controls DiO (5 µM), CFSE (20 µM), or SYTO® (10 µM) were directly added to the cells, so that the same amount of dye was used for EV staining and dye control. Stained cell components and EV uptake were compared to identify non-specific dye transfer from the EV labeling site to the cells. Procedural washing controls (dye in PBS applied to Vivaspin-500 columns) were included to validate the excess dye removal protocol via ultrafiltration columns.

For comparison with liposome uptake Caco-2 cells or Caco-2/HT29-MTX-E12 co-cultures were incubated with the same particle number of DPPC-Chol liposomes or EVmL. When indicated, cells were pre-incubated with 0.25 / 2.5 / 25-fold bovine gamma globulin standard (IgG) (Thermo Scientific, USA) at pH 6 for 30 min. The IgG concentration was adjusted to the total EV protein concentration per well [16]. To investigate temperature-dependent effects, cells were pre-incubated at +4 °C for 30 min prior to EV or liposome incubation as reported by Joshi et al. [31].

2.13 Confocal laser scanning microscopy (CLSM)

Cells were washed thrice with sterile PBS and fixed with 3.7% aqueous formaldehyde. Alexa Fluor™ 568 phalloidin (Thermo Fisher, USA) for F-actin staining and DAPI (4',6-diamidino-2-phenylindole) for nucleus staining were used according to the manufacturer's instructions. Inserts were cut and mounted onto glass cover slips with Fluoromount-G® (SouthernBiotech, USA). Cell uptake was evaluated using a SP8 confocal laser scanning microscope (CLSM) with a 63x/1.40 Oil Plan Apo objective (Leica Microsystems, Wetzlar, Germany). At least 15 images of three independent experiments were acquired in sequential scanning mode for quantitative comparison. Additionally, representative z-stacks were captured for each experiment. Images were processed using the Leica Application Suite (LAS) software and Fiji/ImageJ software. Settings were kept constant for image acquisition and processing.

2.14 EV transport across Caco-2 cells

Transport studies were conducted as described by Hubatsch et al. [24] in accordance with the Food and Drug Administration's (FDA) and European Medicines Agency's (EMA) recommendations [32,33]. In brief, cell culture medium was removed by decanting and transferring the inserts to a new 24-well plate. Cells were washed with sterile Hanks' balanced salt solution (HBSS, with 25 mM HEPES, 4.2 mM $NaHCO_3$) pH 7.4 (basolateral) and pH 6.5 (apical) for 20 min at +37 °C. pH 6.5 for the apical compartment was chosen to mimic the acidic microclimate of the small intestine. Same surface levels of the buffer in the apical and basolateral compartment were ensured to exclude transport effects due to hydrostatic pressure. Cell monolayer integrity was tested with the paracellular permeability marker dextran. FITC-dextran (4 kDa) and Rhod-B-dextran (70 kDa) were dissolved in HBSS pH 6.5 (1 mg · mL^{-1}) and added in parallel to the donor compartment. Concentrations were measured with a plate reader at $\lambda_{ex/em}$ = 487 / 528 nm (FITC) and $\lambda_{ex/em}$ = 554 / 586 nm (Rhod-B) (Synergy H1, BioTek, USA). As a positive control cells were pre-incubated with 2.5 mM EDTA before adding FITC- and Rhod-B-dextrans. Fluorescently labeled EVs were diluted in HBSS pH 6.5 to a final concentration of 1 · 10^{12} particles · mL^{-1} and added to the apical compartment. During transport experiments plates were incubated at +37 °C (no CO_2) on an orbital shaker (100 rpm) to prevent unstirred water layers. Samples were drawn from the apical donor compartment at the beginning (t_0) and end (t_{fin}) of every experiment. Samples from the basolateral acceptor compartment were taken after 15, 30, 45, 60, 90, 120, 240, 360 min for cumulative transport studies or after 1 hour for permeability coefficient calculations. The TEER was measured prior and after each experiment to ensure the cell monolayer intactness.

The trans-epithelial flux was expressed as the apparent permeability coefficient (P_{app}) according to the following equation:

$$P_{app}\ [cm \cdot s^{-1}] = (\delta Q/\delta t) \cdot (1/(A \cdot c_0)) \qquad \text{(equation 3)}.$$

In this equation $\delta Q/\delta t$ is the steady-state flux, A is the surface area of the inserts, and c_0 is the initial concentration in the donor compartment.

The recovery is defined as the sum of EVs recovered from acceptor and donor compartment at the end of the experiment divided by the initial amount in the donor compartment. It is calculated as follows:

$$\text{Recovery}\ [\%] = (c_{D\text{-}fin} \cdot V_{D\text{-}fin} + c_{A\text{-}fin} \cdot V_{A\text{-}fin}) \cdot 100/(c_{D\text{-}0} \cdot V_{D\text{-}0}) \qquad \text{(equation 4)},$$

where V is the volume and c the concentration in the donor (D) or acceptor (A) compartment at the start (0) or end (fin) of the experiment.

EV concentrations were either estimated by fluorescence measurements with a plate reader or by particle measurements with the NTA. For a qualitative evidence of EVs, donor and acceptor aliquots were probed with antibodies against CD63, TSG101 and CD9 as described earlier. Cell controls without EVs were used for background subtraction.

Further control experiments included EV_{DiO} added to cell monolayers differentiated on 0.4 µm inserts and a DiO (5 µM) dye control without EVs.

All transport experiments were performed with $n = 4$.

2.15 Statistical Analysis

All experiments were performed at least in triplicate. Data were analyzed using Origin (Pro), Version 2019 (OriginLab Corporation, Northampton, MA, USA). For comparison of three or more group means, statistical significance was determined by analysis of variance (ANOVA) with Tukey post-hoc test. Results are given as mean ± standard deviation (SD). *P*-values below 0.05 were considered statistically significant and labelled as follows: * for $p < 0.05$, ** for $p < 0.01$, and *** for $p < 0.001$.

3. Results

3.1 EV characterization

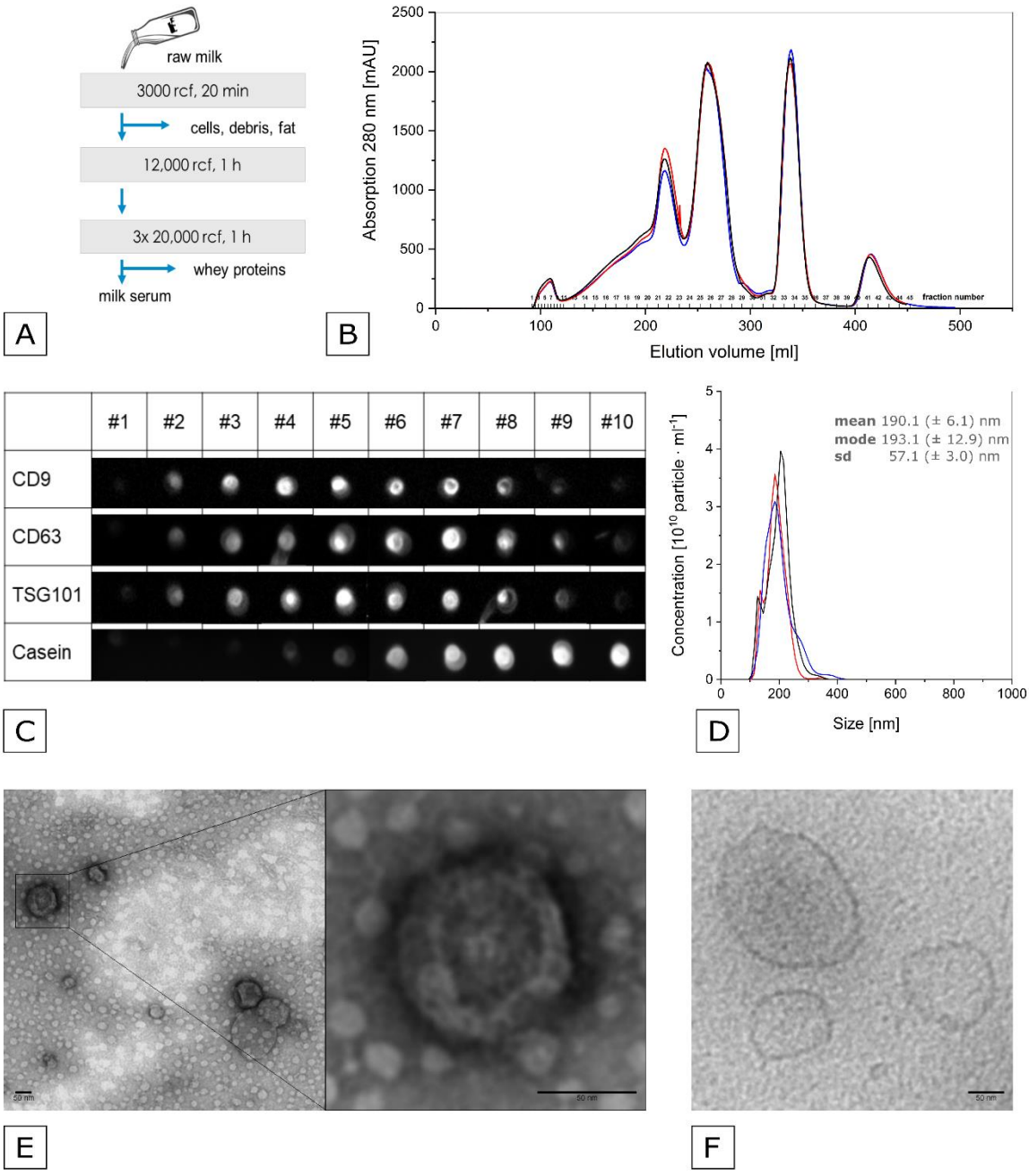

Fig. 1 EV characterization. A, B) Isolation protocol: EVs were enriched from bovine raw milk using a differential centrifugation protocol (A) followed by preparative size-exclusion chromatography (B). The chromatogram shows the elution profile at 280 nm absorbance of three independent runs and the collected fractions. **C) Dot blot:** Aliquots of the eluting fractions 1–10 were probed with antibodies against the EV marker proteins CD9, CD63, Tsg101, and the milk whey contaminant casein. **D) Nanoparticle Tracking Analysis (NTA):** Size distribution was analyzed by NTA (*n* = 3). sd refers to the standard deviation of the size distribution. **E, F) Electron microscopy:** EV morphology was confirmed by

transmission electron microscopy (TEM) (E) and cryoTEM (F). For negative-stained TEM (E) EVs appeared in a characteristic cup-shape due to the dehydration step. A widefield micrograph (left) and a close-up of a single EV (right) are shown. Scale bars represent 50 nm.

To isolate EVs from bovine raw milk a differential centrifugation protocol was applied (***Fig. 1*** *A*) and collected milk serum was further purified and fractionated by size-exclusion chromatography (***Fig. 1*** *B*). The presence of three different EV marker proteins (CD9, CD63, Tsg101) as recommended by the MISEV guidelines [7] was confirmed by antibody detection in fractions 2–9 (***Fig. 1*** *C*). The most abundant milk whey contaminant casein was found in fractions 6–10; in fractions 4–5 its content was neglectable low. For further studies fractions 2–5 were pooled. The size distribution was analyzed on a single particle-based level by Nanoparticle Tracking Analysis (NTA) and ranged between 65 nm and 485 nm with a mean diameter of 190.8 (± 6.1) nm (***Fig. 1*** *D*). A relative standard deviation of 0.30 (± 0.015) can be obtained from the standard deviation (57.1 ± 3.0 nm) given by the NTA software. This relates to a moderate width of the size distribution. The size distribution was consistent with results obtained via a similar SEC isolation protocol [26] but larger than milk EVs isolated via ultracentrifugation and SEC [34] or ultracentrifugation only [35]. The size distribution remained stable over three weeks, when EVs were stored at +4 °C ***(Suppl. 1)***. Nevertheless, only fresh preparations (<5 days) were used for further studies.

Transmission electron microscopy (TEM) showed mainly spherical particles indicating the intactness and high purity of the obtained EVs. For the negative-stained TEM the vesicles appeared in a characteristic cup-shaped morphology [36] due to the drying step during the sample preparation (***Fig. 1*** *E*). CryoTEM confirmed the presence of spherical versicles confined by a well-defined lipid layer, strongly suggesting EVs (***Fig. 1*** *F*).

Quantification	**Method**	**Result (*n* = 3)**
Proteins	Bradford	12.73 (± 0.95) µg · mL^{-1}
Lipids	SPV	7.00 (± 0.01) µg · mL^{-1}
Particles	NTA	6.72 (± 1.1) · 10^{11} particles · mL^{-1}
Particles : Proteins		5.27 (± 1.3) · 10^{10} particles · μg^{-1}
Particles : Lipids		9.60 (± 1.6) · 10^{10} particles · μg^{-1}

Table 1 EVs were quantified regarding proteins using Bradford assay, lipids using Sulpho-Phospho-Vanillin assay (SPV), and particles using nanoparticle tracking analysis (NTA). Particle to protein and particle to lipid ratios were calculated accordingly. Data are shown as mean ± SD; *n* = 3.

EV yield was estimated according to the MISEV 2018 guideline [7] using a Bradford-assay for protein concentration, a Sulpho-Phospho-Vanillin (SPV)-assay for lipid concentration, and NTA for particle concentration (***Table 1***). The particle/protein ratio were consistent with previous published results for milk EVs [26,37]. Cytocompatibility of milk EVs can be assumed as Caco-2 cells incubated with EVs for up to 24 hours showed a cell viability above 80% *(**Suppl. 2***).

3.2 Labeling approaches for EV uptake into intestinal cells

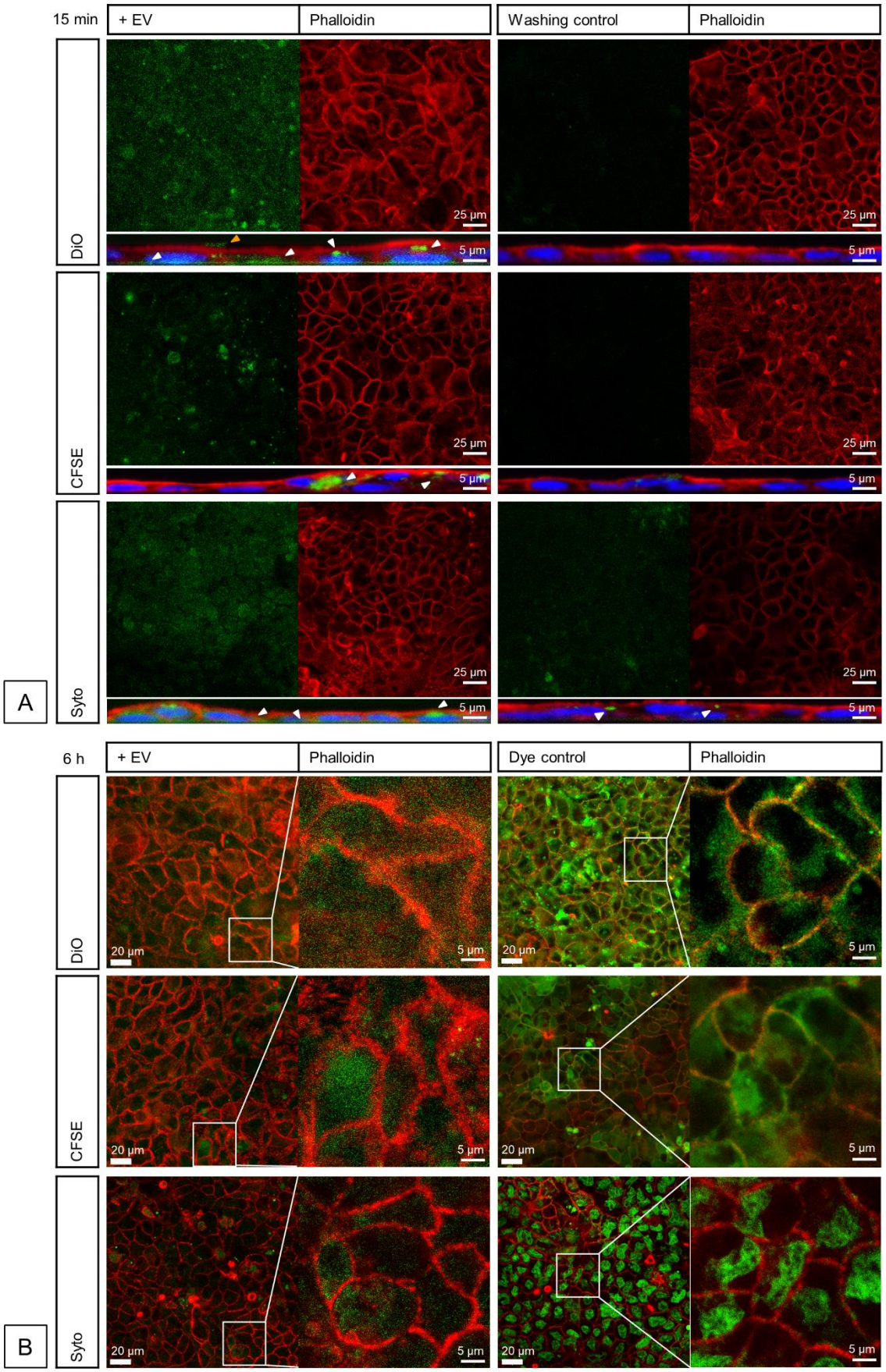

Fig. 2 EV uptake. Representative confocal images at x-y top view are shown. EVs were labeled with DiO for membrane staining, CFSE for protein staining or SYTO® for RNA staining (green). Nuclei were stained with DAPI (blue) and F-actin with Alexa Fluor™ 568 phalloidin (red). **A) Labeling approaches and dye removal:** Caco-2 cells were incubated with labeled EVs for 15 min (left). Corresponding x-z side views (z-stack of 70 images) are shown for each labeling approach. White arrows point towards internalized fluorescence signal, orange arrows towards extracellular fluorescence signal attached to the cell surface. Washing controls without EV (dye in PBS) verify the excess dye removal via ultrafiltration (right). Scale bars indicate 25 µm (x-y top view) or 5 µm (x-z side view) respectively. **B) Dye control after 6 hours:** Caco-2 cells were incubated with labeled EVs for 6 hours (left) and compared to Caco-2 cells directly stained with DiO, CFSE, or SYTO® (right). Differences in the fluorescent signal pattern indicate no or little non-specific dye transfer. Scale bars indicate 20 µm or 5 µm (magnified image) respectively.

Despite emerging labeling techniques [38] EV labeling from commercial bovine milk still needs to rely on exogenous dyes applied post-isolation. Two major drawbacks regarding dyes exist: While excess dye might label cell components, dyes are also reported to undergo a non-specific transfer from their actual EV labeling site to cell components both giving misleading results [17,18].

Excess dye removal

To minimize the risk of seeing dye artefacts we selected three different dyes each staining a distinct cell component: DiO for membranes, CFSE for proteins and SYTO® for RNA. We removed excess dye by adding the stained EVs to ultrafiltration columns (300 kDa MWCO) and washing them thrice with PBS. Dye in PBS undergoing the same ultrafiltration protocol served as a control. Caco-2 cells were incubated with stained EVs for 15 min. Fluorescence signal could be observed with confocal laser scanning microscopy (CLSM) within the cells for all three labeling strategies indicating a fast uptake of EVs into Caco-2 cells (***Fig. 2*** *A, left*). However, fluorescence signal seemed brighter for DiO and SYTO® labeling compared to CFSE labeling. The fluorescence signal was reduced for the SYTO® dye control and no overall signal was detectable for DiO and CFSE dye controls (***Fig. 2*** *A, right*) showing that excess dye was efficiently removed by ultrafiltration.

Non-specific dye transfer

To account for a non-specific dye transfer from EVs to cell components Caco-2 cells were incubated with stained EVs for a longer time period and compared the result to the staining pattern of DiO, CFSE and SYTO® without intermediate ultrafiltration step. Confocal microscopic images of Caco-2 cells with EVs (***Fig. 2*** *B, left*) displayed a distinct fluorescence signal within the cells that differed from the staining

pattern of the cell membrane by DiO, proteins by CFSE, or RNA by SYTO® (***Fig. 2*** *B, right*) after 6 hours. This indicates that little or no non-specific dye transfer from labeled EVs to cell components occurred. However, after 24 hours the fluorescence signal from DiO and SYTO® stained EVs resembled the DiO and SYTO® dye staining pattern (***Suppl. 3***). Therefore, we decided to limit the incubation time to 6 hours for further experiments thus reducing the risk of observing artefacts. Notably, the fluorescence signal from CFSE stained EVs disappeared after 24 hours.

Although we are aware of the pitfalls regarding EV labeling using fluorescent dyes, we are quite convinced to see EV uptake when carefully removing excess dye and limiting the experimental time frame. Using three different labeling approaches adds to the reliability of uptake experiments.

3.3 EV versus liposome uptake into intestinal cells and mechanistic evaluations

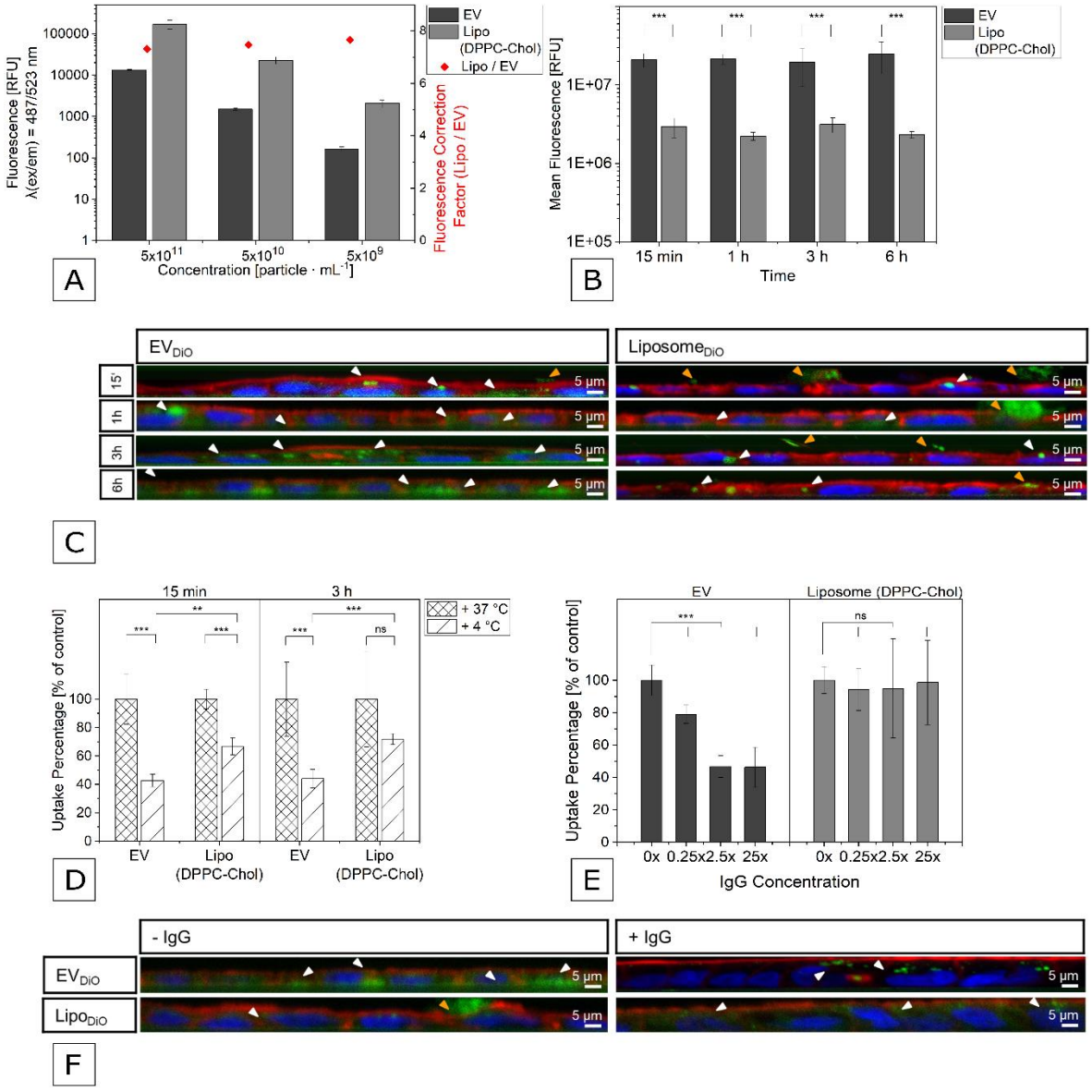

Fig. 3 DPPC-Chol liposomes as uptake controls. A) Fluorescence intensities of DiO labeled EVs and liposomes were compared at different particle concentrations. The ratio of the liposome/EV fluorescence intensity represents the fluorescence correction factor (red square) (*n* = 3). **B)** Fluorescence intensity of EVs was significantly higher than the liposome signal in Caco-2 cells after 15 min, 1 h, 3 h and 6 h (*n* = 3). **C)** Representative confocal images at x-z side views (z-stack of 70 images) of Caco-2 cells incubated with DiO (green) labeled EVs (left) and liposomes (right) are shown. White arrows point towards internalized fluorescence signal, orange arrows towards extracellular fluorescence signal attached to the cell surface. (nuclei: blue, F-actin: red). **D)** To estimate the effect of non-energy-dependent processes EV and liposome uptake was performed at +4 °C for 15 min and 3 h and normalized to controls incubated with EVs or liposomes at +37 °C (*n* = 3). **E)** Caco-2 cells were pre-incubated with a 0.25 / 2.5 / 25-fold IgG concentration to block the FcRn before uptake experiments with EVs and liposomes for 1 h (*n* = 3). Uptake was normalized to controls without IgG pre-treatment incubated with EVs or liposomes. **F)** Z-stacks (70 images) of Caco-2 cells incubated with DiO labeled EVs and liposomes are shown with (left) and without (right) IgG pre-incubation. Scale bars represent 5 µm. Statistical significance is indicated by * for $p < 0.05$, ** for $p < 0.01$, and *** for $p < 0.001$.

Material		**Size [nm]**	**Relative standard deviation**	**Zeta potential [mV]**
EV		190.1 (± 6.1)	0.30 (± 0.015)	–12.2 (± 3.7)
Liposomes	DPPC/Chol (70/30 mol/mol)	195.5 (± 11.5)	0.32 (± 0.027)	–3.1 (± 0.1)
EV mimicking liposomes	DOPC/DOPE/SM/DOPS/Chol (21/17.5/17.5/14/30 mol/mol)	199.9 (± 23.8)	0.30 (± 0.013)	–22.4 (± 0.4)

Table 2 Mean size (NTA), relative standard deviation reflecting the width of the size distribution (NTA), and zeta potential (ELS) of EVs, DPPC-Chol liposomes and EV mimicking liposomes (EVmL). Data are shown as mean ± SD; *n* = 3.

DPPC-Chol liposomes as uptake controls

Liposomes and EVs comprise a common feature, which is a phospholipid bilayer enclosing an aqueous inner core. However, liposomes were being investigated as drug delivery systems for decades and are already established in clinical use [3–5]. The question arose whether bovine milk-derived EVs exhibit superior uptake characteristics in Caco-2 cells compared to standard liposomes (DPPC-Chol 70/30 mol/mol) (***Table 2***).

In fact, CLSM z-stack images after 15 min, 1 h, 3 h and 6 h revealed that liposomes were more likely to attach to the cell surface (blue arrows) whereas EVs were mainly found inside the cells (white arrows) (***Fig.* 3** *C*). Both EVs and liposomes were labeled with DiO and incubation was adjusted to the particle concentration of $2 \cdot 10^{11}$ particles per well for better comparison. Since the labeling efficiency of EVs and liposomes was expected to differ due to different membrane compositions (e.g. different lipid species, membrane proteins in EVs), the fluorescence intensity of stained EVs and liposomes was measured at three different particle concentrations. Liposomes were stained more easily by DiO than EVs. Thus, a fluorescence correction factor of 7.5 (± 0.2) was calculated normalizing the fluorescence of liposomes to that of EVs and applied to further fluorescence measurements (***Fig.* 3** *A*). For quantifying the uptake into Caco-2 cells the mean green channel intensities of 15 CLSM images from three independent experiments were analyzed. Fluorescence intensities were significantly higher for EVs compared to liposomes after all time points (***Fig.* 3** *B*). This contributes to the hypothesis of EVs exhibiting beneficial uptake properties compared to DPPC-Chol liposomes in Caco-2 cells. Remarkably, a time dependent increase in fluorescence could not be observed. Most likely, the uptake appears to be i) considerably fast or ii) saturated with the particle concentration of $2 \cdot 10^{11}$ particles per well. For the latter an active uptake process would be required which has been previously reported in literature previously [14,39].

Energy-dependent uptake

To confirm this, Caco-2 cells were incubated with DiO labeled EVs or liposomes respectively at +4 °C. This is done to mainly mitigate active, receptor-mediated uptake [31] though a temperature decrease also influences the membrane fluidity. Both EV and liposome uptake were decreased at +4 °C compared to +37 °C after 15 min with EV uptake being decreased to a greater extent (***Fig.* 3** *D*). After 3 hours only EV uptake was significantly reduced. Therefore, we conclude that active, temperature-dependent processes are involved in both EV and liposome uptake. However, non-temperature-dependent uptake seems to play a larger role in DPPC-Chol liposomal uptake. Both, active and passive uptake, were further addressed:

The role of the FcRn receptor in EV uptake

Many studies explore various endocytic pathways for EV uptake in different cell types including phagocytosis, clathrin-mediated endocytosis, caveolin-mediated endocytosis, and micropinocytosis [14,39]. Betker et al. proposed an uptake mechanism specific for the internalization in the gastrointestinal system [16]. They found a decreased EV recovery in blood after co-administration of immunoglobulins (IgG) and bovine milk-derived EVs in mice. They attributed this effect to the neonatal Fc receptor (FcRn). The FcRn is known to shuttle immunoglobulins across the intestinal membrane thus

providing an interesting mechanism for the uptake and transport of EVs as well. However, the expression and distribution of the FcRn is highly variable among different species. To shed light in the FcRn uptake involvement in human cells we repeated this study *in vitro*. Caco-2 cells were pre-incubated with a 0.25-, 2.5-, and 25-fold IgG concentration adjusted to the protein concentration of $2 \cdot 10^{11}$ EVs per well. DiO labeled EVs or liposomes were added before the uptake was estimated using CLSM after 1 hour. Z-stack images showed a reduced uptake of EVs whereas liposome uptake seemed unaffected by IgG co-incubation (***Fig.* 3** *F*). When images were quantified regarding their mean green channel intensity (***Fig.* 3** *E*) the liposome uptake remained constant. EV uptake was decreased to 79.0 (± 5.7) percent at a 0.25-fold IgG concentration and further decreased to 46.7 (± 6.6) percent at a higher IgG concentration (2.5-fold). No significant difference between 2.5- and 25-fold IgG concentrations was found indicating a saturation of the FcRn. Accordingly, the FcRn seems to be involved in EV uptake into human Caco-2 cells. Other pathways are likely to contribute to EV uptake as the remaining uptake rate indicates.

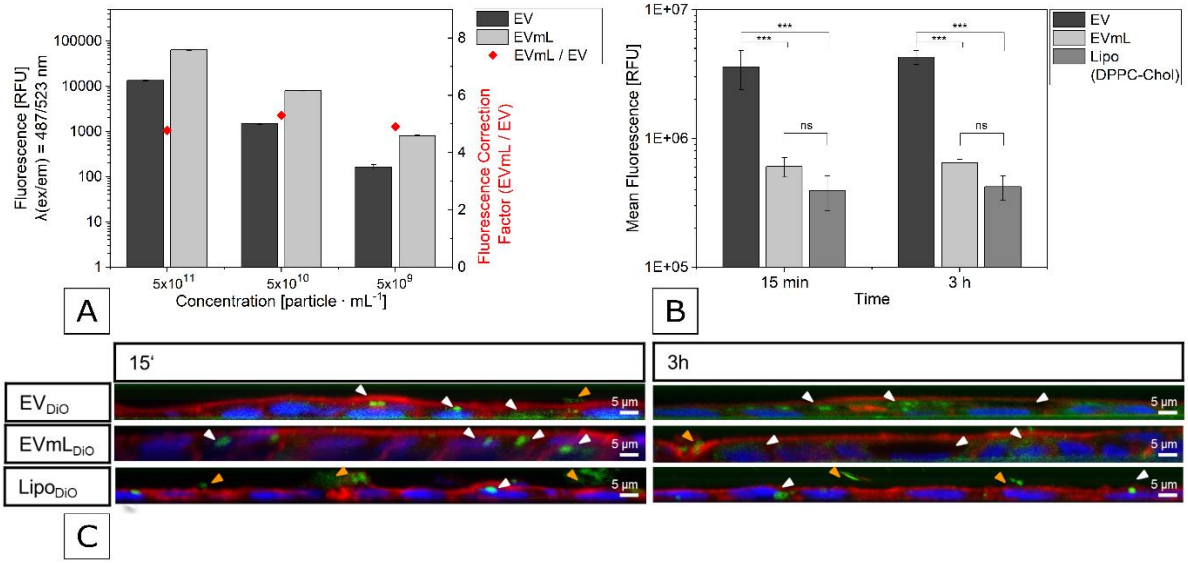

Fig. 4 EV mimicking liposomes (EVmL). A) Fluorescence intensity of DiO labeled EVs and EVmL was compared at different particle concentrations. The ratio of the EVmL/EV fluorescence intensity represents the fluorescence correction factor (red square) (*n* = 3). **B)** EV fluorescence intensity was significantly higher in Caco-2 cells after 15 min and 3 h compared to DPPC-Chol liposomes and EVmL (*n* = 3). **C)** Representative z-stacks of 70 confocal images of Caco-2 cells (nuclei: blue, F-actin: red) incubated with DiO (green) labeled EVs, EVmL and DPPC-Chol liposomes revealed differences between internalized (white arrows) and extracellular fluorescence signals (orange arrows). Scale bars represent 5 µm.

Statistical significance is indicated by * for $p < 0.05$, ** for $p < 0.01$, and *** for $p < 0.001$.

EV mimicking liposomes (EVmL) for passive uptake control

For passive nanoparticle uptake general physicochemical interactions are discussed based on the elasticity model of lipid bilayers introduced by Helfrich [40,41]. The adhesion energy between particles and cell membrane (E_{adh}) is considered to drive the particles into the membrane. The bending and elastic moduli of the membrane (κ) and the membrane surface tension (σ) characterize the cell membrane's resistance to deformation, thereby hindering the engulfment process. Altogether, key factors for passive internalization are the nanoparticle-membrane adhesion energy, the membrane elastic moduli and tension, as well as the charge and size of particles and cells. The lipid composition of liposomes is known to alter this adhesion energy between particles and cell membrane [42]. Therefore, EV mimicking liposomes (EVmL) were prepared according to literature [29] resembling the lipid composition of EVs including a negative zeta potential (***Table 2***). As described previously for the DPPC-Chol liposomes, a fluorescence correction factor was calculated for DiO labeled EVmL at three different concentrations (***Fig. 4*** *A*). The fluorescence correction factor of 5.0 (± 0.3) was applied to fluorescence intensity measurements after incubating Caco-2 cells with EVmL for 15 min or 3 hours (***Fig. 4*** *B*). DiO labeled EVs and DPPC-Chol liposomes were used as controls. Compared to DPPC-Chol liposomes no significant difference in uptake was detectable. EV uptake was significantly higher (approximately 7.5-fold) than the uptake of both DPPC-Chol liposomes and EVmL. However, z-stacks showed less attachment of EVmL to the cell surface compared to DPPC-Chol liposomes (***Fig. 4*** *C*). This may be attributed to the beneficial lipid composition of EVmL.

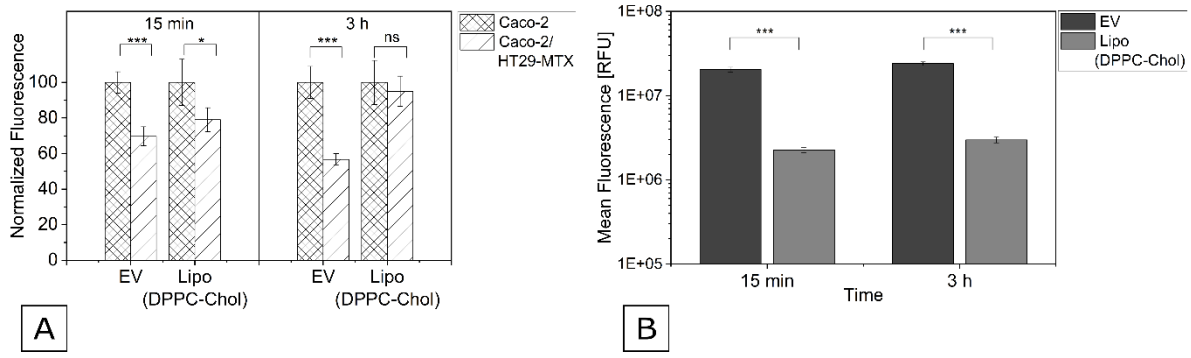

Fig. 5 Uptake across a mucus layer A) EVs and DPPC-Chol liposomes were added to Caco-2/HT29-MTX co-cultured cells for 15 min and 3 h and normalized to Caco-2 controls (n = 15) to estimate the effect of mucopolysaccharides on uptake properties. **B)** Comparison of the overall fluorescence signal between EVs and DPPC-Chol liposomes in Caco-2/HT29-MTX (n = 15). Statistical significance is indicated by * for $p < 0.05$, ** for $p < 0.01$, and *** for $p < 0.001$.

EV uptake across the mucus layer

Though Caco-2 cells are a widely used cell culture model for resorption studies of the upper intestine [21,22], they lack some characteristics of the human intestinal barrier, e.g. gut microbiota, immune cells, intestinal mucus. Especially for nanoparticle uptake goblet cells are relevant. These cells are interspersed between enterocytes where they continuously produce mucus that covers the epithelium. The mucus hinders particles or pathogens to enter the underlying epithelia. Here, we wanted to assess the ability of EVs and liposomes to cross the mucus layer using a Caco-2/HT-29 co-culture [23]. Alcian Blue staining was performed to visualize the mucus production after 21 days of differentiation (***Suppl. 4***). DiO labeled EVs or liposomes (DPPC-Chol) were added to the cells and uptake controlled after 15 min or 3 hours. EV uptake (***Fig. 5*** *A*) was significantly decreased to 69.7 (± 5.4) percent after 15 min and to 56.73 (± 3.30) percent after 3 hours compared to uptake in Caco-2 monoculture. In contrast to that, liposome uptake (***Fig. 5*** *A*) was decreased to a lesser extent to 79.0 (± 6.8) percent after 15 min and no significant effect was measured after 3 hours. The zeta potential (***Table 2***) could explain that EV uptake was hindered to a higher extent compared to liposome uptake. Mucins are glycoproteins composed of a core protein with carbohydrates attached. Acidic mucins (carbohydrates with carboxylate- or sulphonate groups) might lead to electrostatic repulsion of EVs exhibiting a negative zeta potential whereas DPPC-Chol liposomes with a neutral zeta potential remain less affected. In general, the overall uptake of EVs still remained higher than liposome uptake (***Fig. 5*** *B*).

3.4 EV *in vitro* transport across the intestinal barrier

Integrity of the Caco-2 monolayer

Transport across the Caco-2 monolayer is a Food and Drug Administration (FDA) and European Medicines Agency (EMA) approved method to estimate the drug permeability *in vitro* [32,33] but careful method validation and quality controls are necessary to obtain reliable results. Firstly, confocal microscopy after F-actin staining visualized that cells were growing in a monolayer. Secondly, the integrity of the monolayer was monitored by TEER measures prior and after the experiment [32] and we excluded cell monolayers with TEER values below 255 $\Omega \cdot cm^2$. Thirdly, compounds with zero permeability are recommended as an additional integrity control [32]. We selected fluorescently labeled dextrans (4 kDa and 70 kDa) as hydrophilic paracellular markers. Permeability coefficients of 3.6 (± 0.6) $\cdot 10^{-8}$ cm $\cdot s^{-1}$ for FITC-Dextran 4 kDa and 1.7 (± 0.9) $\cdot 10^{-8}$ cm $\cdot s^{-1}$ for Rhod-B-Dextran 70 kDa were obtained for intact cell layers. When tight junctions were disrupted with EDTA, compromised cell layers showed a 13- to 56-fold increase in dextran permeability (***Suppl.*** **5**).

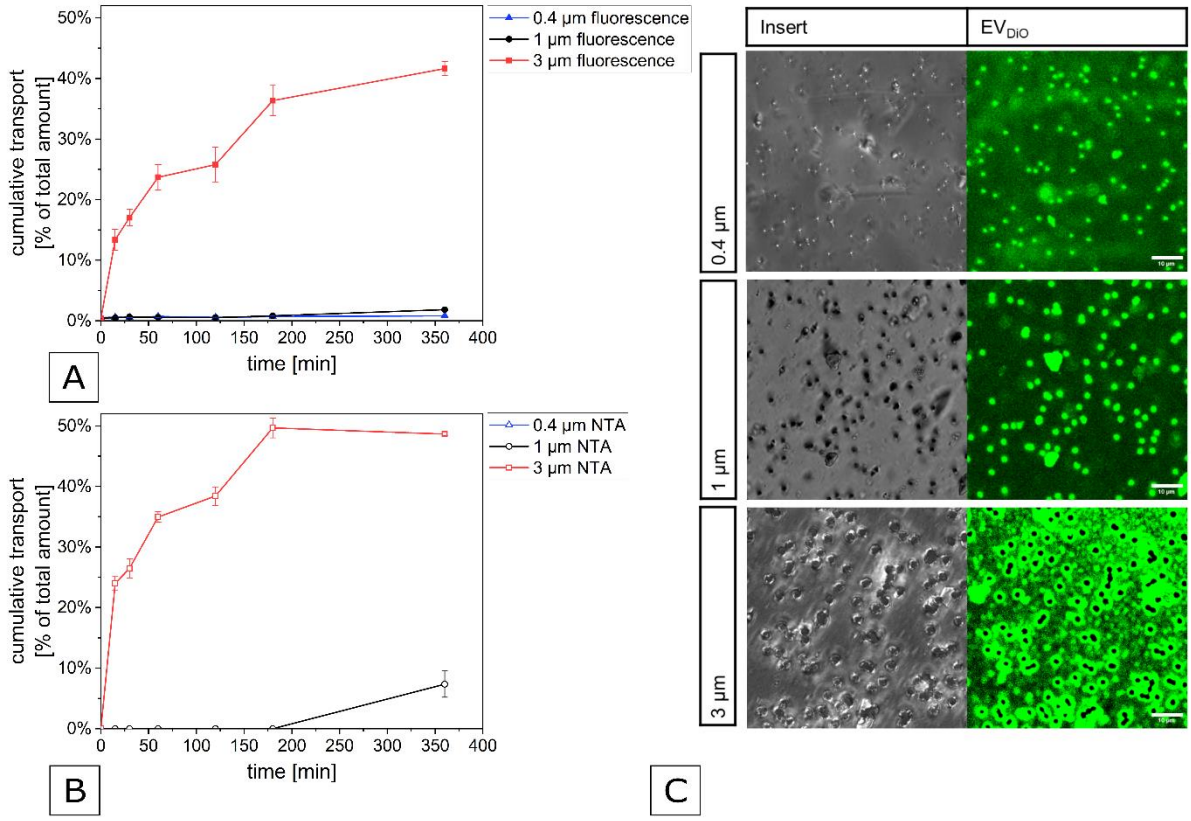

Fig. 6 Pre-tests on insert pore size determination. A-B) DiO labeled EVs were added to inserts with pore sizes of 0.4, 1, or 3 µm and the cumulative transport calculated after fluorescence measurements (A) and NTA (B) (*n* = 3). **C)** Confocal images of insert surfaces (top view from the donor side) after incubation with DiO labeled EVs (green) show clogged pores for 0.4 µm and 1 µm inserts. Scale bars represent 10 µm.

Pre-testing the optimal insert pore size for EV transport

Additional standardization approaches include the choice of buffer, pH, cell culture inserts, shaking, sampling time, and a limited cell passage number [22,24,25]. However, these standards were published for small molecules and need to be carefully evaluated for EV transport studies. From our perspective, the most critical recommendation is the insert pore size. Usually, a pore size of 0.4 µm is advised to prevent cells from entering the pores and growing at the insert bottom [24]. We could demonstrate that larger pore sizes of 3 µm are required for EV transport. DiO labeled EVs were added to the donor compartment of inserts with 0.4, 1, or 3 µm pores. The cumulative transport reached 41.6 (± 1.2) percent for 3 µm inserts after 6 hours whereas the cumulative transport remained low with 0.8 (± 0.1) percent for 0.4 µm inserts and 1.8 (± 0.5) percent for 1 µm inserts (***Fig. 6*** *A*). Similar results were obtained when the cumulative transport of particles was measured by NTA (***Fig. 6*** *B*). As visualized by CLSM imaging the pores of 3 µm inserts remained free of fluorescence signal at the donor side (top view) from EVs after incubation (***Fig. 6*** *C*). In contrast, smaller pores were clogged by EVs. At

the same time, when Caco-2 cells were seeded on 3 µm inserts, no cells were found at the insert bottom. This indicates no migration of Caco-2 cells through the pores contributing to the applicability of these inserts.

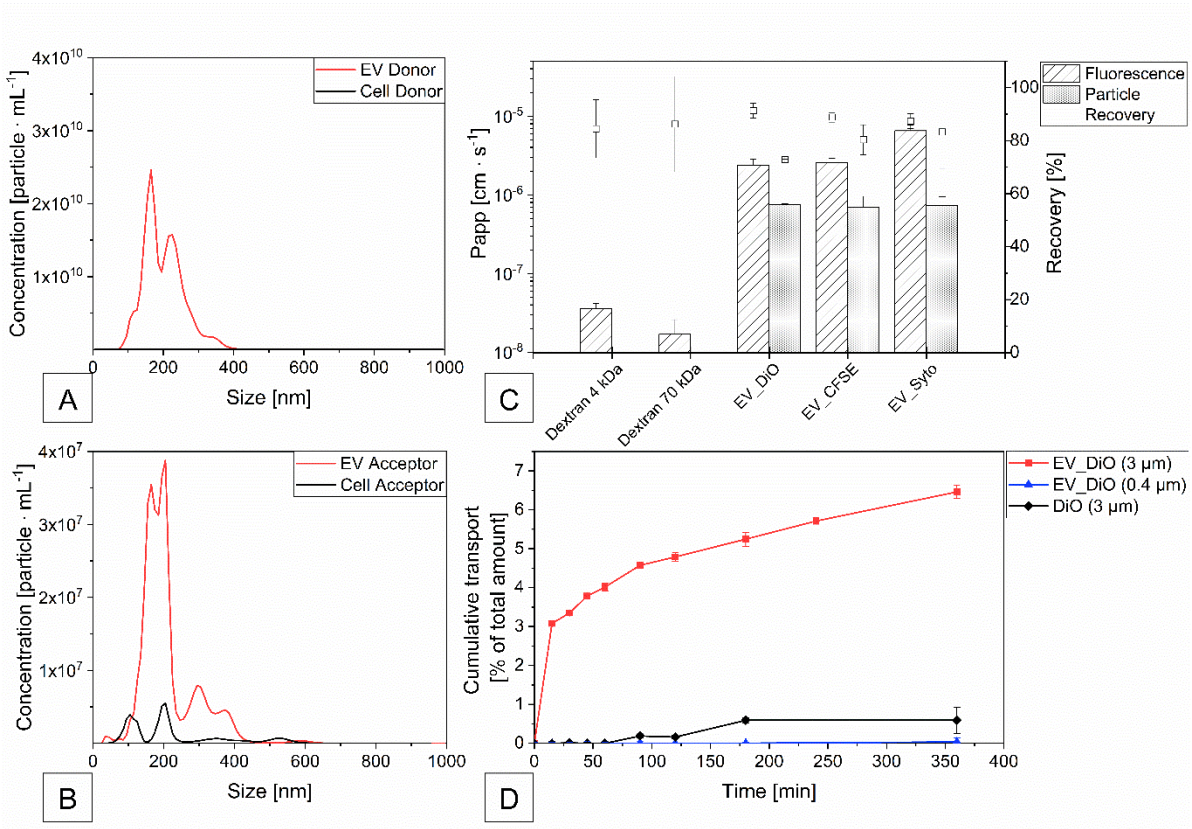

Fig. 7 EV transport across Caco-2 monolayers. A-B) Representative NTA measurements in the donor (A) and acceptor (B) compartment for cell controls (black) and cells incubated with EVs (red) for 1 h (*n* = 3). **C)** Apparent permeability coefficients (P_{app}) and recovery rates were calculated by means of fluorescence for dextrans as permeability markers and fluorescently labeled EVs and by means of particle concentrations for EVs (*n* = 4). Cell controls were used for background subtraction. **D)** Cumulative transport of DiO labeled EVs across Caco-2 cells on inserts with a pore size of 0.4 µm (blue) and 3 µm (red) is shown. DiO only (black) was used as a control (Caco-2 cells on inserts with a pore size of 3 µm) (*n* = 3).

Apparent permeability coefficient (P_{app})

The apparent permeability coefficient (P_{app}) is used to compare drug permeability *in vitro*. The drug concentration in the acceptor compartment is analyzed after a defined sampling time. Bovine milk-derived EVs are less applicable to standard analysis techniques (e.g. HPLC, UV-Vis, fluorescence). The fact that Caco-2 cells are shedding EVs themselves during the experiments further complicates transport studies.

We decided to analyze inherent features, the size distribution and particle concentration via NTA and protein markers via antibody detection, as well as exogenous labels used for prior uptake studies to guarantee for most reliable results. However, antibody detection was not sensitive enough to detect differences of EV markers in the acceptor compartment between cells incubated with EVs and controls (***Suppl. 6***).

Particle concentration measurements revealed particles in both donor and acceptor compartment of cells incubated with EVs after 1 hour (***Fig. 7*** *A–B*). Cell controls without EVs also showed particles in the size range of bovine milk-derived EVs in the acceptor compartment (***Fig. 7*** *B*) but not in the donor compartment (***Fig. 7*** *A*). For P_{app} calculations cell control concentrations were subtracted resulting in a permeability coefficient of 7.3 (± 0.3) · 10^{-7} cm · s^{-1} which was significantly higher than the permeability of paracellular dextran markers (***Fig. 7*** *C*).

Three different fluorescent labeling approaches (DiO, CFSE, and SYTO®) showed comparable P_{app} values of 2.4 (± 0.4) · 10^{-6} cm · s^{-1} for EV_{DiO} and 2.6 (± 0.3) · 10^{-6} cm · s^{-1} for EV_{CFSE} and a slightly higher P_{app} value of 6.5 (± 1.2) · 10^{-6} cm · s^{-1} for $EV_{Syto®}$ (***Fig. 7*** *C*). Permeability coefficients obtained from particle concentrations were similar for all three labeling strategies (***Fig. 7*** *C*).

To ensure that EVs and not dissociated dye were transported across the cell monolayer, DiO-labeled EVs were added to Caco-2 cells seeded on 0.4 µm inserts. As shown before EVs are retained by 0.4 µm pore sizes. Indeed, the cumulative transport rate was found to be only 0.03 (± 0.11) percent across Caco-2 cells on 0.4 µm inserts for EV_{DiO} after 6 hours *(**Fig. 7*** *D*). Dye only showed a similarly low cumulative transport of 0.6 (± 0.3) percent when added to Caco-2 cells on 3 µm inserts whereas EV_{DiO} were cumulatively transported to 6.5 (± 0.2) percent across Caco-2 cells on 3 µm inserts (***Fig. 7*** *D*). This leads to the assumption that in fact EVs are transported.

4. Discussion

Bovine milk-derived EVs hold promises for oral drug delivery due to their scalable production [13], gastrointestinal stability [9,10], and uptake properties [14,16]. However, the hurdles regarding milk EVs are rarely addressed:

Bovine milk is a complex biological fluid which contains – besides EVs – fat droplets, cell debris and soluble proteins (e.g. casein micelles) [43]. This makes it challenging to isolate EVs of high purity and low batch-to-batch variability. Here, we could successfully isolate EVs using a two-step isolation protocol with differential centrifugation followed by a highly consistent, preparative SEC. EVs were analyzed regarding their morphology and purity (TEM, CryoTEM) and monitored for size distribution and particle concentration (NTA), proteins (Bradford, dot blot), lipid concentration (SPV), and zeta potential (ELS) to get reproducible EV preparations (***Fig. 1***).

Another challenge is the labeling necessary to track EV uptake and transport. Though progresses in EV labeling techniques were made, including GFP or luciferase reporter proteins fused to CD63 [38,44], this attempt is mainly limited to EVs produced by genetically modified cell cultures. Bovine milk-derived EVs need to be labeled post isolation. A recent study introduced a ^{99m}Tc (IV) label for single photon emission computed tomography (SPECT) imaging of EVs in mice [19]. However, access to radiation-based techniques is not widely available in most research labs. Copper-free click-chemistry based surface protein labeling is another approach [20]. Nevertheless, further studies are required to exclude disruption of surface epitopes and alterations of biological properties due to the reaction conditions.

Therefore, we selected fluorescent dyes for EV labeling although two drawbacks are reported. Firstly, excess dye could label cell components and secondly, a non-specific transfer from the actual EV labeling site to cell components might occur [17,18]. To identify the strategy with the least dye artefacts, three different labeling sites were addressed including DiO for membranes, CFSE for proteins, and SYTO® for RNA thereby increasing the reliability of uptake and transport results. Removal of excess dye via ultrafiltration was validated with dye in PBS undergoing the same washing procedure. A fast EV uptake within 15 min was observed by CLSM with dye controls showing extremely weak to no detectable fluorescence signal (***Fig. 2*** *A*). Thus, ultrafiltration was feasible to remove excess dye.

Non-specific dye transfer was analyzed using free dye controls. A recent ISEV position paper recommends the use of free dye controls for experiments with stained EVs [45]. Indeed, the fluorescence staining pattern of cell components from DiO and SYTO® was similar to the one from labeled EVs after 24 hours in Caco-2 cells. Remarkably, the EV staining pattern differed after 6 hours indicating little or no non-specific dye transfer (***Fig. 2*** *B*). The fading signal of CFSE stained EVs after

24 hours might be attributed to a low fluorescence intensity at pH<7 when EVs undergo endocytosis [46]. This approach allows only for a qualitative comparison of the dye distribution pattern. The quantitative information is limited as the total dye amount in the EV preparation and the dye control are not identical because excess dye was removed from the EVs via ultrafiltration steps. One idea might be to quantify dye release from EVs without cells. However, this proofed difficult because the dyes used exhibit a different fluorescence emission upon binding to the respective cell components compared to free dyes. Therefore, the incubation time was limited to 6 hours to cover the physiological relevant time span in the gastrointestinal system and to prevent the risk of artefacts due to non-specific dye transfer at the same time. Altogether, we could show that removal of excess dye via ultrafiltration and a limited incubation time frame are suitable to circumvent pitfalls reported for labeling strategies with fluorescent dyes.

With these conditions set for a reliable fluorescent EV labeling, we characterized and standardized EV bioavailability *in vitro* regarding cell uptake and transport across the intestinal barrier model.

The uptake properties of bovine milk-derived EVs were directly compared to liposomes. Liposomes are well-investigated and market-authorized drug delivery systems and resemble EVs in terms of size and morphology, characterized by an aqueous inner core enveloped by a phospholipid membrane. This makes them an ideal candidate to investigate a potential uptake superiority of EVs into intestinal cells. A previous *in vitro* study for example showed that porphyrin loaded EVs significantly reduced the cell viability of MDA cells through phototoxicity upon laser irradiation while liposomes had no effect [47]. *In vivo* experiments found evidence that doxorubicin-loaded EVs reduced the tumor volume more effectively than liposomes after intratumoral injection [48]. To the best of our knowledge, no *in vitro* head-to head comparisons between bovine milk-derived EVs and liposomes in intestinal cells have been performed so far. Market-authorized lipid formulations mainly composed of phosphatidylcholine and cholesterol are considered a fair and relevant control [3,6]. On this basis, we selected DPPC-Chol liposomes (70/30 mol/mol). In fact, bovine milk-derived EVs outperformed standard liposomes in terms of uptake efficiency in Caco-2 cells used to model the intestinal barrier (***Fig.* 3** *B,C*) when normalized to the particle concentration. However, we found differences in the labeling efficiency between EVs and liposomes. We accounted for this by introducing a novel fluorescence correction factor (***Fig.* 3** *A*) that enhances the comparability. Our investigations revealed that most EV uptake was temperature dependent. This points towards an active, receptor-mediated uptake [14,31] although membrane fluidity effects might also appear at low temperatures. A receptor-mediated uptake is in agreement with earlier reports which found clathrin- and caveolae-dependent endocytosis involved in cellular uptake of bovine milk-derived EVs [14,39]. More specifically, the FcRn was proposed as key for EV absorption from the gastrointestinal system of mice [16]. As the expression and distribution of the

FcRn varies remarkably between different species we analyzed the role of the FcRn for EV and liposome uptake for the first time in a human cell line. Of note, the blocking of the FcRn decreased the uptake of EVs whereas liposomal uptake remained unaffected (***Fig.* 3** *E,F*). Non-energy-dependent uptake seemed to be more influential in liposome uptake. Here, cell internalization could be improved by changing the lipid composition. Still, EV uptake remained higher than EVmL uptake. This correlates with a report that found EVmL uptake ranked between standard liposomes and cationic liposomes [29].

Oral bioavailability of macromolecules and nanoparticles is considerably limited by the intestinal mucus spanning the intestinal epithelium. To simulate these conditions, a co-culture model of Caco-2 and goblet-like HT29-MTX cells was used [23]. Though the overall uptake of EVs compared to liposomes was still higher, EV uptake was partially hindered by the mucus layer. This might be attributed to electrostatic repulsion between EVs that have a negative zeta potential and acidic mucins. Surface PEGylation of EVs showed a higher mucus permeability compared to native EVs tested with native porcine intestinal mucus in an earlier study [37] and could be a possible strategy to further enhance the mucus penetration of milk-derived EVs.

Though the uptake mechanism of EV into intestinal cells is not fully elucidated, we conclude that bovine milk-derived EVs exhibit beneficial uptake properties compared to liposomes in the cell lines used. FcRn was found as one pathway exclusive for EV uptake in Caco-2 cells. Future studies should investigate differences regarding the functional delivery capacity of EVs and liposomes. Uptake might not necessarily be equivalent to the release of therapeutic cargo from the endosome to the desired compartment. Alterations between results obtained in cell line models (e.g. Caco-2 and HT29-MTX) and primary cells or more advanced intestinal models also need to be considered. Apart from that, a fluorescence correction factor might be useful for a more direct comparison of EVs and liposomes in the future.

Finally, a standardized method for EV transport across the Caco-2 monolayer was established. Though *in vivo* studies confirming the bioavailability of bovine milk-derived EVs exist [9,15], several questions remain unsolved. One report found different biodistribution patterns for infrared-labeled microRNAs loaded into bovine milk-derived EVs in mice after oral administration [15]. While this would indicate a transfer of cargo from milk-derived EVs to endogenous EVs the authors also found accumulation of non-loaded milk-derived EVs in the brain. This leads to the question whether EVs stay intact when crossing the intestinal barrier. Another study fed mice with locked nucleic acid-modified antisense oligonucleotide (LNA ASOs) loaded bovine milk-derived EVs via oral gavage. However, they recovered only 1% of the administered dose and observed no functional effect [9]. Here, *in vitro* transport studies could be beneficial as a fast screening method before starting *in vivo* experiments for drug delivery via

bovine milk-derived EVs. Additionally, P_{app} values allow for easier comparison of bioavailability tests compared to complex *in vivo* experimental set ups.

Transport studies across the Caco-2 monolayer are used to estimate the drug permeability *in vitro* and are approved by regulatory authorities (e.g. FDA, EMA) [32,33]. However, method validation and quality controls for reliable results were established for small molecules. We could demonstrate that the insert pore size is crucial for the experimental set up with EVs. Unlike previous reports on *in vitro* EV transport [37,49,50], our findings strongly suggest inserts with 3 µm pores to be able to recover EVs with a mean diameter of 190.1 (± 6.1) nm in the donor compartment (***Fig. 6***). Regularly used inserts with 0.4 µm pores are blocked by EVs of this size range thus preventing any EV transport from the donor to the acceptor compartment. TEER measurements and paracellular markers (dextran 4 kDa and 70 kDa) were used to confirm the integrity of the epithelial layer throughout the experiments and prevent any misinterpretation of damage to the Caco-2 layer as apparent transport. Further standards including buffer, pH, volume, incubation time and shaking frequency for drug delivery across Caco-2 cells from established [24,25] and authorized [32,33] protocols for small molecules were applied.

Despite a thoroughly controlled set up the detection of bovine milk-derived EVs in the acceptor compartment remained challenging as the Caco-2 cells produce EVs themselves. Previous studies used EV associated cargo to circumvent this problem [14,50]. However, cargo transport and EV transport might not necessarily correspond. In a recent ISEV position paper arising from the ISEV membranes and EVs workshop most agree that it is not possible to generate cells or animals free of producing any vesicles [45]. Therefore, including cell controls is necessary when investigating inherent features of EVs like proteins or particle concentration in the donor compartment. In our case, antibody detection of EV marker proteins was not sensitive enough to show differences between EV treated cell monolayers and controls. However, particle concentration and fluorescence measurement with three labels gave P_{app} values of $0.7–6.5 \cdot 10^{-6}$ cm $\cdot$ s^{-1} (***Fig. 7****)* which were significantly higher than the transport rate of cell impermeable dextrans ($1.7–3.6 \cdot 10^{-8}$ cm $\cdot$ s^{-1}). With two complementary methods giving permeability coefficients within the same magnitude, we confirmed that EVs are indeed transported across the Caco-2 monolayer. Particle concentration measurements however lead to slightly lower P_{app} values compared to P_{app} values obtained from fluorescence measurements. Here, fluorescence is considered the more accurate method due to higher sensitivity and a higher linear range that saves up dilution steps needed for NTA. In addition, the recovery rate found for particle measurements was significantly lower (73–83 percent) compared to fluorescence measurements (87–91 percent) (***Fig. 7*** *C*) which also impacts the P_{app} value. Higher recovery rates lead to a lower error of the permeability coefficient [24]. In literature, apparent permeability coefficients of $2–5 \cdot 10^{-6}$ cm $\cdot$ s^{-1} are obtained for

rapidly transported compounds [24] which covers the range of 2.4–6.5 · 10^{-6} cm · s^{-1} we obtained as P_{app} values by fluorescence measurements for bovine milk-derived EVs.

Still, one limitation of apparent permeability coefficients is their translation for *in vivo* experiments. For market-authorized small molecules correlation curves between P_{app} values from Caco-2 transport experiments and absorbed fractions in humans after oral administration exist [51]. This allows for a good estimation of the bioavailability of new drugs once the P_{app} value is determined. Future studies need to determine whether these correlation curves apply for EVs as well.

So far, the apparent bioavailability of bovine milk-derived EVs is reported to be 3.9 (± 2.1) percent after 3 hours and 5.9 (± 2.6) percent after 24 hours in mice when comparing the DiR signal after oral gavage compared to intravenous administration [15]. This correlates well with the cumulative transport rate of 6.5 (± 0.2) percent across Caco-2 cells we found after 6 hours (***Fig. 7** D*). Controls with free dye showed only a cumulative transport rate of 0.6 (± 0.3) percent. When labeled EVs were added to Caco-2 cells on 0.4 µm inserts the transport rate was limited to 0.03 (± 0.11) percent (***Fig. 7** D*). Therefore, we conclude that EVs and not dissociated dye were transported across the Caco-2 monolayer.

5. Conclusion

In this work, uptake and transport across the intestinal barrier as two key factors for EV bioavailability were critically investigated.

We demonstrated the beneficial uptake properties of bovine milk-derived EVs compared to liposomes in intestinal cell models in a head-to-head comparison. This was possible by applying a fluorescence correction factor that accounts for different labeling efficiencies. Though the mechanisms for internalization are not yet fully elucidated, the FcRn receptor provides an uptake pathway exclusive for EVs in human cells. EVmL show slightly improved internalization properties compared to DPPC-Chol liposomes. Both EVs and liposomes permeate the intestinal mucus. Beforehand, the suitability of EV staining was proofed using a limited time frame to minimize non-specific dye transfer, excess dye removal via ultrafiltration, and three distinct labeling sites.

We also provided a standardized protocol for transport studies across Caco-2 monolayers with respect to EV requirements, thus allowing for a fast *in vitro* screening. To the best of our knowledge, we were the first to report P_{app} values for EVs reflecting the transport rate. P_{app} values obtained with this model will add to the comparability of future bioavailability testings and can serve as a basis for rationally designed EV therapeutics.

Acknowledgement

The authors kindly acknowledge Prof. Achim Aigner and Dr. Alexander Ewe (Rudolf-Boehm-Institute, Clinical Pharmacology, Leipzig) for access to the NTA instrument, Prof. Annette Beck-Sickinger and Isabelle Ziffert (Biochemistry and Bioorganic Chemistry, Leipzig) for their support with the dot blot analysis, and PD Dr. Dr. John T. Heiker (Biochemistry, Leipzig) for providing the ÄKTA instrument.

Declaration of competing interest

None.

References

[1] P. Lundquist, P. Artursson, Oral absorption of peptides and nanoparticles across the human intestine: Opportunities, limitations and studies in human tissues, Advanced drug delivery reviews 106 (2016).

[2] C.M. O'Driscoll, A. Bernkop-Schnürch, J.D. Friedl, V. Préat, V. Jannin, Oral delivery of non-viral nucleic acid-based therapeutics - do we have the guts for this?, European Journal of Pharmaceutical Sciences 133 (2019) 190–204.

[3] D.J.A. Crommelin, P. van Hoogevest, G. Storm, The role of liposomes in clinical nanomedicine development. What now? Now what?, Journal of controlled release official journal of the Controlled Release Society 318 (2020) 256–263.

[4] Food and Drug Administration, Approval Letter for AmBisome (amphotericin B) Liposome for Injection (1997).

[5] Food and Drug Administration, Liposome Drug Products: Chemistry, Manufacturing, and Controls; Human Pharmacokinetics and Bioavailability; and Labeling Documentation: Guidance for Industry (2018).

[6] K.B. Johnsen, J.M. Gudbergsson, M. Duroux, T. Moos, T.L. Andresen, J.B. Simonsen, On the use of liposome controls in studies investigating the clinical potential of extracellular vesicle-based drug delivery systems – A commentary, Journal of Controlled Release 269 (2018) 10–14.

[7] C. Théry, K.W. Witwer, E. Aikawa, M.J. Alcaraz, J.D. Anderson, et al., Minimal information for studies of extracellular vesicles 2018 (MISEV2018): a position statement of the International Society for Extracellular Vesicles and update of the MISEV2014 guidelines, Journal of extracellular vesicles 7 (2018) 1535750.

[8] M. Yáñez-Mó, P.R. Siljander, Z. Andreu, A.B. Zavec, F.E. Borràs, et al., Biological properties of extracellular vesicles and their physiological functions, Journal of extracellular vesicles 4 (2015).

[9] P. Grossen, M. Portmann, E. Koller, M. Duschmalé, T. Minz, et al., Evaluation of Bovine Milk Extracellular Vesicles for the Delivery of Locked Nucleic Acid Antisense Oligonucleotides, European journal of pharmaceutics and biopharmaceutics official journal of Arbeitsgemeinschaft fur Pharmazeutische Verfahrenstechnik e.V (2020).

[10] Y. Liao, X. Du, J. Li, B. Lönnerdal, Human milk exosomes and their microRNAs survive digestion in vitro and are taken up by human intestinal cells, Molecular nutrition & food research 61 (2017).

[11] M. Somiya, Y. Yoshioka, T. Ochiya, Biocompatibility of highly purified bovine milk-derived extracellular vesicles, Journal of extracellular vesicles 7 (2018).

[12] A. Matsuda, A. Moirangthem, R.S. Angom, K. Ishiguro, J. Driscoll, I.K. Yan, D. Mukhopadhyay, T. Patel, Safety of bovine milk derived extracellular vesicles used for delivery of RNA therapeutics in zebrafish and mice, Journal of applied toxicology JAT (2019).

[13] R. Munagala, F. Aqil, J. Jeyabalan, R.C. Gupta, Bovine milk-derived exosomes for drug delivery, Cancer letters 371 (2016) 48–61.

[14] T. Wolf, S.R. Baier, J. Zempleni, The Intestinal Transport of Bovine Milk Exosomes Is Mediated by Endocytosis in Human Colon Carcinoma Caco-2 Cells and Rat Small Intestinal IEC-6 Cells, The Journal of nutrition 145 (2015) 2201–2206.

[15] S. Manca, B. Upadhyaya, E. Mutai, A.T. Desaulniers, R.A. Cederberg, B.R. White, J. Zempleni, Milk exosomes are bioavailable and distinct microRNA cargos have unique tissue distribution patterns, Scientific reports 8 (2018) 11321.

[16] J.L. Betker, B.M. Angle, M.W. Graner, T.J. Anchordoquy, The Potential of Exosomes from Cow Milk for Oral Delivery, Journal of pharmaceutical sciences 108 (2019) 1496–1505.

[17] J.B. Simonsen, Pitfalls associated with lipophilic fluorophore staining of extracellular vesicles for uptake studies, Journal of extracellular vesicles 8 (2019) 1582237.

[18] K. Takov, D.M. Yellon, S.M. Davidson, Confounding factors in vesicle uptake studies using fluorescent lipophilic membrane dyes, Journal of extracellular vesicles 6 (2017) 1388731.

[19] M.I. González, P. Martín-Duque, M. Desco, B. Salinas, Radioactive Labeling of Milk-Derived Exosomes With 99m Tc and In Vivo Tracking by SPECT Imaging, Nanomaterials (Basel, Switzerland) 10 (2020).

[20] L. Xu, F.N. Faruqu, R. Liam-Or, A.O. Abu, D. Li, et al., Design of experiment (DoE)-driven in vitro and in vivo uptake studies of exosomes for pancreatic cancer delivery enabled by copper-free click chemistry-based labelling, Journal of extracellular vesicles 9 (2020).

[21] P. Stenberg, U. Norinder, K. Luthman, P. Artursson, Experimental and Computational Screening Models for the Prediction of Intestinal Drug Absorption, Journal of Medicinal Chemistry 44 (2001) 1927–1937.

[22] T. Jarc, M. Novak, N. Hevir, T.L. Rižner, M.E. Kreft, K. Kristan, Demonstrating suitability of the Caco-2 cell model for BCS-based biowaiver according to the recent FDA and ICH harmonised guidelines, The Journal of pharmacy and pharmacology 71 (2019).

[23] E. Walter, S. Janich, B.J. Roessler, J.M. Hilfinger, G.L. Amidon, HT29-MTX/Caco-2 cocultures as an in vitro model for the intestinal epithelium: in vitro-in vivo correlation with permeability data from rats and humans, Journal of pharmaceutical sciences 85 (1996).

[24] Ina Hubatsch, Eva G E Ragnarsson, Per Artursson, Determination of drug permeability and prediction of drug absorption in Caco-2 monolayers, Nat Protoc 2 (2007) 2111–2119.

[25] M. Natoli, B.D. Leoni, I. D'Agnano, F. Zucco, A. Felsani, Good Caco-2 cell culture practices: The LIINTOP project: Optimisation of liver and intestine in vitro models for pharmacokinetics and pharmacodynamics studies, Toxicology in Vitro 26 (2012) 1243–1246.

[26] K. Blans, M.S. Hansen, L.V. Sørensen, M.L. Hvam, K.A. Howard, A. Möller, L. Wiking, L.B. Larsen, J.T. Rasmussen, Pellet-free isolation of human and bovine milk extracellular vesicles by size-exclusion chromatography, Journal of extracellular vesicles 6 (2017) 1294340.

[27] T. Westergard, B. K. Jensen, X. Wen, J. Cai, E. Kropf, et al., Cell-to-Cell Transmission of Dipeptide Repeat Proteins Linked to C9orf72-ALS/FTD, Cell Reports 17 (2016) 645–652.

[28] T. Visnovitz, X. Osteikoetxea, B.W. Sódar, J. Mihály, P. Lőrincz, K.V. Vukman, E.Á. Tóth, A. Koncz, I. Székács, R. Horváth, Z. Varga, E.I. Buzás, An improved 96 well plate format lipid quantification assay for standardisation of experiments with extracellular vesicles, Journal of extracellular vesicles 8 (2019) 1565263.

[29] M. Lu, X. Zhao, H. Xing, Z. Xun, S. Zhu, L. Lang, T. Yang, C. Cai, D. Wang, P. Ding, Comparison of exosome-mimicking liposomes with conventional liposomes for intracellular delivery of siRNA, International journal of pharmaceutics 550 (2018) 100–113.

[30] A. Béduneau, C. Tempesta, S. Fimbel, Y. Pellequer, V. Jannin, et al., A tunable Caco-2/HT29-MTX co-culture model mimicking variable permeabilities of the human intestine obtained by an original seeding procedure, European Journal of Pharmaceutics and Biopharmaceutics 87 (2014) 290–298.

[31] B.S. Joshi, M.A. de Beer, B.N.G. Giepmans, I.S. Zuhorn, Endocytosis of Extracellular Vesicles and Release of Their Cargo from Endosomes, ACS nano 14 (2020) 4444–4455.

[32] Food and Drug Administration, M9 Biopharmaceutics Classification System-based Biowaivers: ICH Harmonised Guideline (2018).

[33] European Medicines Agency, Guideline on the investigation of drug interactions: CPMP/EWP/560/95/Rev. 1 Corr. 2** (2012).

[34] L. del Pozo-Acebo, López de las Hazas, M-C, J. Tomé-Carneiro, P. Gil-Cabrerizo, R. San-Cristobal, R. Busto, A. García-Ruiz, A. Dávalos, Bovine Milk-Derived Exosomes as a Drug Delivery Vehicle for miRNA-Based Therapy, International journal of molecular sciences 22 (2021).

[35] M. Somiya, Y. Yoshioka, T. Ochiya, Biocompatibility of highly purified bovine milk-derived extracellular vesicles, Journal of extracellular vesicles 7 (2018).

[36] L.G. Rikkert, R. Nieuwland, Terstappen, L. W. M. M., F.A.W. Coumans, Quality of extracellular vesicle images by transmission electron microscopy is operator and protocol dependent, Journal of extracellular vesicles 8 (2019).

[37] Warren, C. Zhang, A. Vedadghavami, K. Bokvist, P.K. Dhal, A.G. Bajpayee, Milk exosomes with enhanced mucus penetrability for oral delivery of siRNA, Biomaterials science (2020).

[38] Y.-J. Li, J.-Y. Wu, J.-M. Wang, X.-B. Hu, D.-X. Xiang, Emerging strategies for labeling and tracking of extracellular vesicles, Journal of controlled release official journal of the Controlled Release Society 328 (2020) 141–159.

[39] F. Aqil, R. Munagala, J. Jeyabalan, A.K. Agrawal, R. Gupta, Exosomes for the Enhanced Tissue Bioavailability and Efficacy of Curcumin, The AAPS journal 19 (2017).

[40] C. Contini, M. Schneemilch, S. Gaisford, N. Quirke, Nanoparticle–membrane interactions, Journal of Experimental Nanoscience 13 (2018) 62–81.

[41] W. Helfrich, Elastic properties of lipid bilayers: theory and possible experiments, Zeitschrift fur Naturforschung. Teil C: Biochemie, Biophysik, Biologie, Virologie 28 (1973).

[42] M.E. Haque, T.J. McIntosh, B.R. Lentz, Influence of Lipid Composition on Physical Properties and PEG-Mediated Fusion of Curved and Uncurved Model Membrane Vesicles: “Nature’s Own” Fusogenic Lipid Bilayer, Biochemistry 40 (2001) 4340–4348.

[43] P.F. Fox, P.L.H. McSweeney, Dairy Chemistry and Biochemistry, First edition ed., Thomson Science, London, 1998.

[44] D. Gupta, X. Liang, S. Pavlova, O.P.B. Wiklander, G. Corso, et al., Quantification of extracellular vesicles in vitro and in vivo using sensitive bioluminescence imaging, Journal of extracellular vesicles 9 (2020).

[45] A.E. Russell, A. Sneider, K.W. Witwer, P. Bergese, S.N. Bhattacharyya, et al., Biological membranes in EV biogenesis, stability, uptake, and cargo transfer: an ISEV position paper arising from the ISEV membranes and EVs workshop, Journal of extracellular vesicles 8 (2019) 1684862.

[46] X. Zhou, J. Zhang, Z. Song, S. Lu, Y. Yu, J. Tian, X. Li, F. Guan, ExoTracker: a low-pH-activatable fluorescent probe for labeling exosomes and monitoring endocytosis and trafficking, Chemical communications (Cambridge, England) 56 (2020).

[47] G. Fuhrmann, A. Serio, M. Mazo, R. Nair, M.M. Stevens, Active loading into extracellular vesicles significantly improves the cellular uptake and photodynamic effect of porphyrins, Journal of controlled release official journal of the Controlled Release Society 205 (2015) 35–44.

[48] T. Smyth, M. Kullberg, N. Malik, P. Smith-Jones, M.W. Graner, T.J. Anchordoquy, Biodistribution and delivery efficiency of unmodified tumor-derived exosomes, Journal of Controlled Release 199 (2015) 145–155.

[49] G. Carobolante, J. Mantaj, E. Ferrari, D. Vllasaliu, Cow Milk and Intestinal Epithelial Cell-derived Extracellular Vesicles as Systems for Enhancing Oral Drug Delivery, Pharmaceutics 12 (2020).

[50] M. Vashisht, P. Rani, S.K. Onteru, D. Singh, Curcumin Encapsulated in Milk Exosomes Resists Human Digestion and Possesses Enhanced Intestinal Permeability in Vitro, Appl Biochem Biotechnol 183 (2017) 993–1007.

[51] P. Artursson, J. Karlsson, Correlation between oral drug absorption in humans and apparent drug permeability coefficients in human intestinal epithelial (Caco-2) cells, Biochemical and biophysical research communications 175 (1991).

Appendix A. Supplementary material

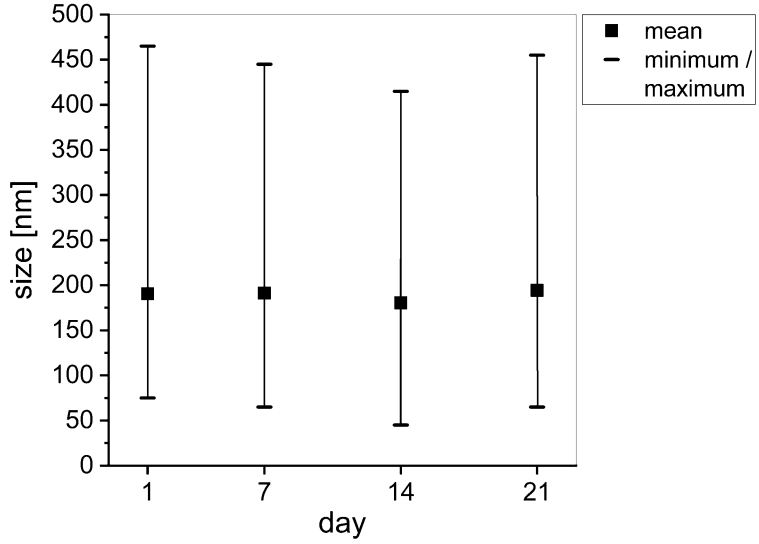

Suppl. 1 EV size over 21 days. EVs stored at +4 °C remained stable regarding their mean, minimum, and maximum size as determined by NTA. Minimum and maximum thresholds were set at concentrations of 1 x 10^6 particles · mL^{-1}.

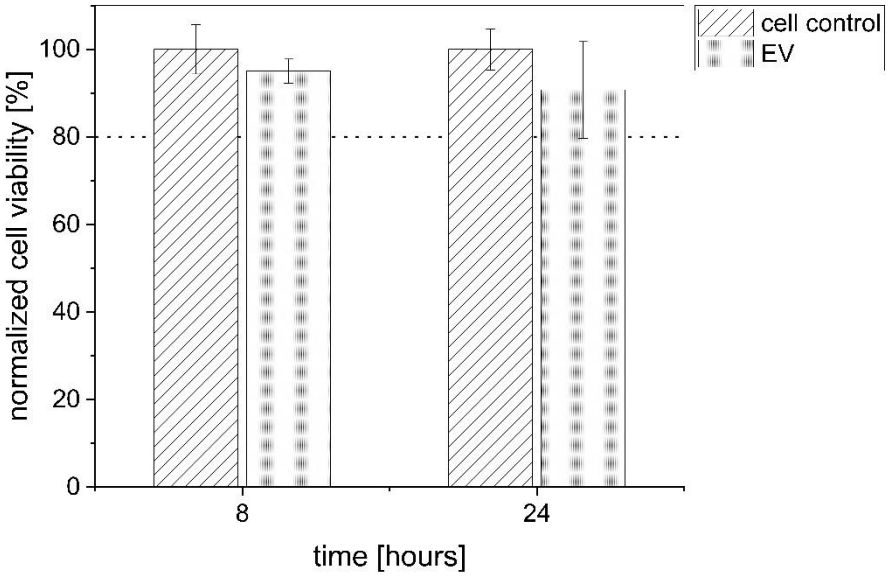

Suppl. 2 Cell viability. Caco-2 cells incubated with milk EVs for 8 and 24 hours showed a cell viability above 80% compared to non-treated Caco-2 cells.

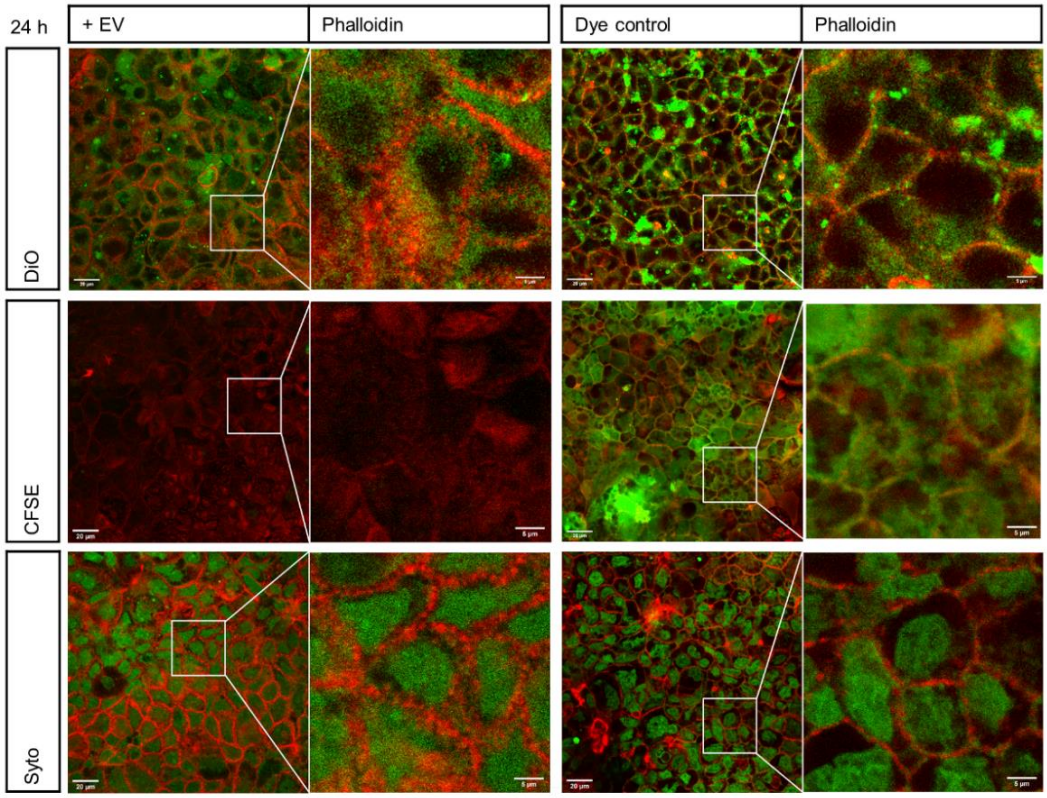

Suppl. 3 Dye control after 24 hours. Caco-2 cells were incubated with labeled EVs for 24 hours (left) and compared to Caco-2 cells directly stained with DiO, CFSE, or SYTO® (right). DiO and SYTO® signal distributions are similar between EVs and dye control indicating that non-specific dye transfer might have occurred. F-actin was stained with Alexa Fluor® 568 phalloidin (red). Scale bars represent 20 µm or 5 µm (magnified image) respectively.

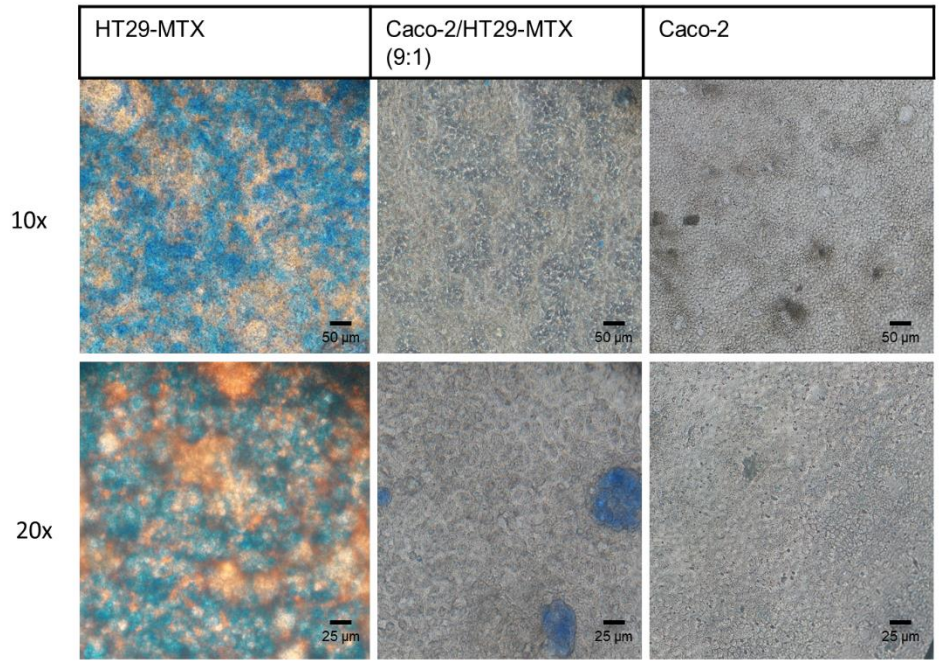

Suppl. 4 Alcian Blue staining of acidic mucins Light microscopy at 10x and 20x magnification of HT29-MTX, Caco-2/HT29-MTX (9:1) and Caco-2 reveals the Alcian Blue staining of acid mucopolysaccharides (blue). Scale bars represent 50 µm (10x) or 25 µm (20x) respectively.

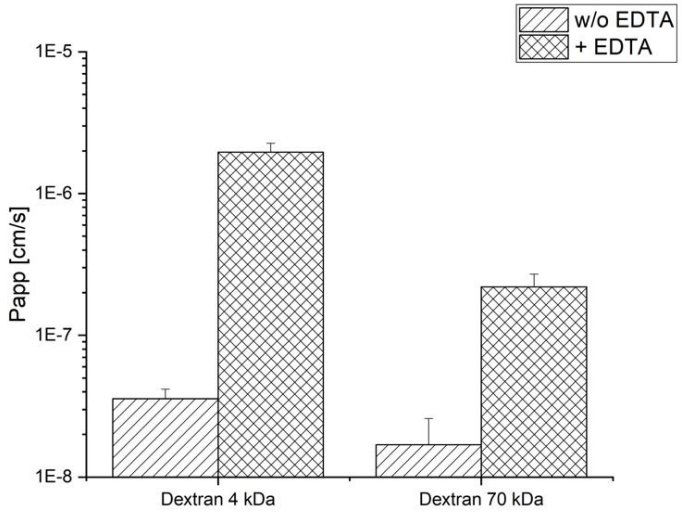

Suppl. 5 P_{app} of Dextran. P_{app} of Dextran (4 kDa and 70 kDa) increases when the cell layer is disrupted with EDTA indicating an intact cell layer in the first place (*n* = 4).

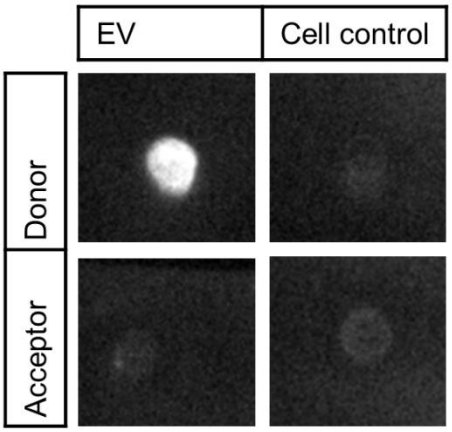

Suppl. 6 Dot blot analysis after transport experiments. Aliquots of the donor and acceptor compartment after transport experiments were probed with antibodies against the EV marker protein CD63. Antibody detection was not sensitive enough to detect differences between acceptor compartments of EVs and cell controls.